Two-field and single-field representations of gas–solid reactive flow with surface reactions

Ivan Girault, Amine Chadil, Enrica Masi, Stéphane Vincent, Olivier Simonin

Two-field and single-field representations of gas-solid reactive flow with surface reactions

Ivan Girault[a,b], Amine Chadil[b,*], Enrica Masi[a], Stéphane Vincent[b], Olivier Simonin[a]

[a] *Institut de Mécanique des Fluides de Toulouse (IMFT), Université de Toulouse, CNRS, Toulouse, 31400, France*
[b] *CNRS, Univ Gustave Eiffel, Univ Paris-Est Créteil, UMR 8208, MSME, Marne-La-Vallée, 77454, France*

Abstract

A single-field representation is derived to describe a multi-species gas flow seeded with perfectly rigid, non-porous and partially inert particles. Indeed, the latter are not involved in heterogeneous reactions with the gas phase (no consumption of the solid by the gas), but they are expected to potentially undergo adsorption and recombination of gaseous radicals on their surface, resulting in the desorption of stable species into the gas. In this work, integral balances are first established at the gas-solid interface, consistent with the local single-phase equations for reactive multi-species gas flow. This allows rigorous derivation of the jump equations that apply at the gas-solid interface in the presence of surface reactions. Then, the description in terms of local single-phase equations, completed by the jump equations at the interface, is recast into a set of equations for the full domain in the sense of distributions. The result extends Kataoka's formalism [I. Kataoka, International Journal of Multiphase Flow 12 (5) (1986) 745–758] to reactive gas-solid flow in the presence of both homogeneous and surface reactions.

Keywords: two-field and single-field representations, reactive flow, gas-solid flow, PR-DNS, surface reactions, combustion

*Corresponding author

Email addresses: ivan.girault@imft.fr (Ivan Girault), amine.chadil@cnrs.fr (Amine Chadil), enrica.masi@imft.fr (Enrica Masi), stephane.vincent@univ-eiffel.fr (Stéphane Vincent), olivier.simonin@toulouse-inp.fr (Olivier Simonin)

Nomenclature

Generic variables

ϕ	two-phase scalar field
$\boldsymbol{\phi}$	two-phase vector field
$\hat{\phi}$	surface scalar field
$\hat{\boldsymbol{\phi}}$	surface vector field
Θ	two-phase scalar source term
$\boldsymbol{\Theta}$	two-phase vector source term
$\hat{\Theta}$	surface scalar source term
$\hat{\boldsymbol{\Theta}}$	surface vector source term
$\mathbf{J}$	two-phase diffusion flux of a scalar quantity
$\boldsymbol{J}$	two-phase diffusion flux of a vector quantity
$\hat{\mathbf{J}}$	surface diffusion flux of a scalar quantity
$\hat{J}$	surface scalar field representing the surface diffusion of a vector quantity

Two-phase fields

β	thermal expansion coefficient	K^{-1}
χ_T	isothermal compressibility coefficient	Pa^{-1}
$\chi^{(m)}$	indicator function of phase $\mathcal{P}^{(m)}$	
κ	bulk viscosity	$\mathrm{Pa\,s}$
λ	thermal conductivity	$\mathrm{W\,m^{-1}\,K^{-1}}$
μ	shear viscosity	$\mathrm{Pa\,s}$
$\dot{\omega}_k$	mass reaction rate of species k per unit volume	$\mathrm{kg\,s^{-1}\,m^{-3}}$
$\dot{\omega}'_T$	heat rate due to homogeneous reactions per unit volume	$\mathrm{W\,m^{-3}}$
ρ	density	$\mathrm{kg\,m^{-3}}$
$\boldsymbol{\sigma}$	total stress tensor	Pa
$\boldsymbol{\tau}$	viscous stress tensor	Pa
C_p	mass heat capacity at constant pressure	$\mathrm{J\,K^{-1}\,kg^{-1}}$
$\boldsymbol{e}$	rate-of-strain tensor	$\mathrm{s^{-1}}$
e_t	mass total energy	$\mathrm{J\,kg^{-1}}$
P	pressure	Pa
h	mass enthalpy	$\mathrm{J\,kg^{-1}}$
$\dot{\mathcal{Q}}$	heat rate due to radiative transfer per unit volume	$\mathrm{W\,m^{-3}}$
$\mathbf{q}$	total heat flux	$\mathrm{W\,m^{-2}}$

T	temperature	K
$\mathbf{u}$	velocity	$\mathrm{m\,s^{-1}}$
$\mathbf{V}_k$	diffusion velocity of species k	$\mathrm{m\,s^{-1}}$
W	molar mass	$\mathrm{kg\,mol^{-1}}$
X_k	molar fraction of species k	
Y_k	mass fraction of species k	

Surface fields (variables with a hat)

$\hat{\Gamma}$	density of surface sites	$\mathrm{mol\,m^{-2}}$
$\dot{\hat{\omega}}_k$	mass rate of species k per unit surface	$\mathrm{kg\,s^{-1}\,m^{-2}}$
$\hat{\rho}$	surface density	$\mathrm{kg\,m^{-2}}$
$\hat{\rho}_k$	surface density of species k	$\mathrm{kg\,m^{-2}}$
$\hat{e}$	mass internal energy	$\mathrm{J\,kg^{-1}}$
$\hat{\mathcal{L}}_T$	interfacial source term in the temperature equation	$\mathrm{J\,m^{-2}}$
$\hat{\mathbf{n}}^{(m)}$	normal vector to the interface Σ directed outwards from the phase $\mathcal{P}^{(m)}$	
$\dot{\hat{\mathcal{Q}}}$	heat rate due to radiative transfer per unit surface	$\mathrm{W\,m^{-2}}$
$\dot{\hat{Q}}_j$	molar rate of the jth surface reaction per unit surface	$\mathrm{mol\,s^{-1}\,m^{-2}}$
$\dot{\hat{s}}_k$	molar rate of species k per unit surface	$\mathrm{mol\,s^{-1}\,m^{-2}}$
$\dot{\hat{s}}_*$	molar rate of vacant sites $*$ per unit surface	$\mathrm{mol\,s^{-1}\,m^{-2}}$
$\hat{\mathbf{w}}$	velocity of the gas-solid interface Σ	$\mathrm{m\,s^{-1}}$
$\widehat{[X_k]}$	molar density of species k per unit surface	$\mathrm{mol\,m^{-2}}$
$\widehat{[X_*]}$	molar density of vacant sites $*$ per unit surface	$\mathrm{mol\,m^{-2}}$
$\hat{Z}_k$	fraction of surface sites occupied by the species k	
$\hat{Z}_*$	fraction of vacant sites	

Geometric quantities related to the material volume Fig. 1

∂V	surface surrounding the material volume V	$\mathrm{m^2}$
$\partial(V^{(m)})$	surface surrounding the volume $V^{(m)}$	$\mathrm{m^2}$
$(\partial V)^{(m)}$	intersection between the phase m and the surface ∂V	$\mathrm{m^2}$
$\mathcal{C}$	contour circling the surface $\mathcal{S}$	m
$\mathcal{S}$	intersection between the material volume V and and the interface Σ	$\mathrm{m^2}$
$\hat{\mathbf{N}}$	surface vector normal to $\mathcal{C}$, tangent to Σ, directed outwards $\mathcal{S}$	
V	material volume	$\mathrm{m^3}$
$\mathbf{n}^{(m)}$	normal vector to the surface $\partial(V^{(m)})$	

$V^{(m)}$	intersection between the volume V and the phase m	m^3

Properties of chemical species and vacant surface sites

σ_k	site occupancy number of species k	
C_{pk}	mass heat capacity at constant pressure of species k	$\mathrm{J\,K^{-1}\,kg^{-1}}$
e_k	mass internal energy of species k	$\mathrm{J\,kg^{-1}}$
$e_{\mathrm{mol},*}$	molar internal energy of vacant sites *	$\mathrm{J\,mol^{-1}}$
h_k	mass enthalpy of species k	$\mathrm{J\,kg^{-1}}$
$h_{\mathrm{mol},*}$	molar enthalpy of vacant sites *	$\mathrm{J\,mol^{-1}}$
W_k	molar mass of species k	$\mathrm{kg\,mol^{-1}}$

Other symbols

$\delta(x)$	1D Dirac distribution	$[x]^{-1}$
δ_Σ	surface Dirac distribution associated with the interface Σ	m^{-1}
ν'_{kj}	molar stoechiometric coefficient of reacting species k in surface reaction j	
ν'_{*j}	molar stoechiometric coefficient of reacting surface sites in surface reaction j	
ν''_{kj}	molar stoechiometric coefficient of produced species k in surface reaction j	
ν''_{*j}	molar stoechiometric coefficient of produced surface sites in surface reaction j	
$\Omega^{(1)}$	set of gas species	
$\Omega^{(2)}$	set of solid species	
$\Omega^{(\Sigma)}$	set of surface species	
Σ	solid-gas interface	
f	function defining the position of the interface Σ	
$\mathbf{g}$	gravity	$\mathrm{m\,s^{-2}}$
H	Heaviside function	
j	index for the surface reactions	
K	total number of gas, solid and surface species	
k	index for species	
k_s	index for the unique solid species	
$\mathcal{M}_k$	molecule of species k	
$\mathcal{M}_*$	vacant surface site	
M_Σ	number of surface reactions	
m	index for phases	
$\mathcal{P}^{(1)}$	gas phase	
$\mathcal{P}^{(2)}$	solid phase	

1. Introduction

Gas-solid reactive flows are increasingly used in industrial applications to convert energy in a clean way, such as in chemical looping combustion technology [35]. They are also found in conventional industrial processes for the production of materials such as synthetic polymers, iron or steel, which are now being redesigned to reduce greenhouse gas emissions [5]. Many of the applications that aim at contributing to industrial decarbonation use the fluidized bed concept [41]. Industrial design and optimization of fluidized bed reactors can be advantageously supported by numerical simulation rather than by building prototypes: it is cheaper, any new geometry of reactor can be easily investigated, and numerical simulation provides data inside the device that are hardly or not accessible through experimental investigation. However, at the scale of an industrial reactor, the current computing power only allows solving Eulerian-Lagrangian systems of equations using parcels instead of particles [50, 44], or Eulerian-Eulerian averaged equations where particles are considered as a continuum, such as in the Euler-Euler approach (or Two-Fluid Model) [22, 28]. Focusing on the latter, the averaged equations for both phases feature unclosed terms that need to be modeled [48]. Thus, the reliability of these numerical simulations to predict the reactive flow depends on the models and on the accuracy of the closure laws used in such an approach.

To develop these closures, a *multiscale approach* can be adopted [6]. It consists in performing simulations at a scale smaller than the one needing closures, among the available scales. Each scale corresponds to a different level of modeling, which is then used to extract information and develop closure models by an *a priori* analysis. Considering the particle resolution as a starting point (and not the pore), and a three-dimensional framework, three scales may be identified. The *microscopic scale* where the flow is resolved at the scale of the individual particle. Conservation equations are directly solved, with resolved jump conditions describing the momentum, mass, and energy transfers between the gas and the dispersed phase. The solid particles are considered as perfectly rigid. Only particle-particle and particle-wall collisions are modeled (generally with a soft-sphere model), as well as lubrication effects in the small unresolved gaps. Such simulations are termed as *Particle-Resolved Direct Numerical Simulations* (PR-DNS) [16]. The *mesoscopic scale* where the flow is no longer resolved at the scale of the individual particle (typically in the boundary layer) but rather modeled by accounting for the effects of the interactions between the fluid and the particles contained in a volume of control in an averaged way. Solid collisions are however directly computed with either a soft-sphere [55] or a hard-sphere model [27]. Averaged equations for mass, momentum, and energy conservation are solved to describe the gas phase, together with equations modeling the multispecies reactive gas phase and the turbulent flow when needed. All interactions between the continuous and dispersed phases are modeled through closure laws, which can be provided by using, for example, PR-DNS. In the literature, this method ([15, 54]) is mainly referred to as *Discrete Element Method* (DEM). The *macroscopic scale* in which both the continuous and the dispersed phases are described, for example, as interpenetrating media. Averaged equations are solved for each phase. High-order moments (gas and particle kinetic energies, fluid-particle covariance, gas turbulent dissipation, etc.) are often used to model the unresolved gas-solid mixture, accounting for the interphase coupling effects. Compared to DEM, additional models based on the kinetic theroy for granular flow [31] are necessary to describe the dispersed phase, as well as particle-particle and particle-wall interactions [30]. Such an approach is the aforementioned *Euler-Euler approach* or *Two-Fluid Model* (TFM). In a multiscale approach, closures may be provided using PR-DNS [52, 26] or CFD-DEM [42] results.

This study is part of a project that aims at characterizing and modeling hydrogen combustion in fluidized beds through a multiscale approach (micro versus macroscale modeling). Hydrogen combustion takes place in a reactor filled with partially inert particles, which may undergo adsorption and recombination of gaseous radicals on their surfaces, resulting in the desorption of stable species to the gas. In this regard, their modeling is needed even at the microscopic scale. The development of a theoretical formalism accounting for surface reactions at microscopic scale is the goal of the present study. This work is therefore concerned with the PR-DNS approach of such systems.

Several numerical methods exist in the literature to perform PR-DNS. In the last years, the community has essentially focused on fixed grid strategies, and among them, we can cite:

- *Immersed Boundary Methods* (IBM), that comprise the method proposed by Uhlmann [56] and enhanced by Breugem [7], *the Ghost Cell Method* [38] and *the Cut Cell method* [46].

- *Fictitious domain methods*, which comprise *the Fictitious-Domain Discrete-Lagrange-Multipliers* (FD-DLM) [24, 47] and *the Viscous Penalty Method* (VPM) [57, 11].

For an exhaustive review of numerical methods for PR-DNS, the reader is referred to the references [40, 58].

This article focuses on the previously mentioned VPM. This method has been shown to accurately describe heat and momentum transfers between an incompressible fluid and a fixed array of spherical particles [10, 52, 12]. It has also been used to successfully reproduce an experimental liquid-solid fluidized bed [43]. The VPM is based on the resolution of a one-fluid formulation on a fixed Cartesian grid, where the solid particles are described as a fluid with infinite viscosity. To the best of our knowledge, no one-fluid formulation accounting for homogeneous and surface reactions is available in the literature.

A one-fluid formulation is a set of spatially averaged equations describing the two-phase flow as a single equivalent fluid. It has mainly been applied in the litterature to gas-liquid and liquid-liquid flows. In these contexts, examples of rigorous derivations are described in [59, 39, 36, 21, 18, 37]. For a more thorough review of applications of the one-fluid formulation in the litterature, the reader can refer to [53]. One-fluid formulation should not be confused with the *single-field representation* introduced by Kataoka [33]; a single-field representation is a set of equations in the sense of distributions describing the evolution of physical quantities, that is rigorously equivalent to the separate single-phase and jump equations at the interface, for each quantity. In fact, a one-fluid formulation is as a spatially averaged single-field representation, that takes the numerical smoothing of discontinuities at the two-phase interface into account. In this regard, our goal is to establish the fundamental single-field representation describing reactive gas-solid flow in the presence of surface reactions.

The article is organized as follows. In Sec. 2, the theoretical framework, notations and physical assumptions concerning the description of the gas-solid reactive flow are introduced. In Sec. 3 the two-field representation is presented. This part focuses on the rigorous derivation of the jump conditions at the gas-solid interface using integral balances, following the approach of [19]. The local single-phase equations are also recalled. Then, in Sec. 4 the local single-phase and jump equations are embedded into the single-field representation in the sense of distributions, extending the work of Kataoka [33] to the reactive gas-solid flows accounting for surface reactions. Conclusions and perspectives are finally outlined.

2. Assumptions, notations and fundamental relations

This section states the assumptions considered in this study. Physical and modeling assumptions are first presented in Sec. 2.1. Definitions, conventions, and notations are then progressively introduced in Secs. 2.2, 2.3, 2.4 and 2.5.

2.1. Assumptions

The solid particles are supposed to be partially inert in the following sense: they are not consumed by heterogeneous reactions or phase change, but the gas-solid interface can undergo surface processes, involving adsorption of unstable gaseous radicals on the surface, recombination of these radicals into stable molecules, followed by the desorption of these molecules in the gas phase. The particles are also supposed to be made of a perfectly non-porous solid. They are modeled as a Newtonian incompressible fluid with an infinite shear viscosity, and a thermal expansion coefficient equal to zero.

The gas-solid interface is described as a sharp material dividing surface. It is composed of surface sites where gaseous species can adsorb. It is supposed to feature a single type of surface site. The local density of sites is considered to be constant over the surface of the particles, and independant of time. Note that this is a simplified view of the real surface chemistry, as it may exist different types of adsorption sites (terrace sites, step sites, etc.), with different thermo-chemical properties and whose local density can vary (see the references [34, 51] for more details). Moreover, the adsorbed species are supposed to be non-interacting molecules (perfect mixture), and it is assumed that the state of the resulting surface phase does not depend on the state of the adjacent bulk phases; the surface phase is said *autonomous* [17], which is a very simplifying assumption knowing the molecular-size thickness of the surface phase. These two last assumptions follow the ideal surface model implemented in the Surface Chemkin [13] and Cantera [25] software. Additionally, we assume the continuity of both the temperature and tangential component of the velocity at the interface. All

phenomena related to surface diffusion are neglected. Finally, the mechanical effects due to surface tension are neglected because of the rigid character of the solid.

The reactive gas mixture is described with the conservation equations of [45]. Gravity is the only external force.

2.2. Domains and phases

In the formalism adopted by Cantera [25], and introduced by Kee *et al.* [34], the gas-solid flow is divided into three *domains*: i) gas, ii) bulk solid, and iii) gas-solid interface. Note that the gas and bulk solid are *volume* domains, while the gas-solid interface is a *surface* domain.

In this formalism, each domain can then feature an arbitrary number of "phases". In our problem, each domain features in fact only one "phase". The gas domain only contains the gas. The bulk solid domain only contains homogeneous condensed matter, due to the assumption of non-porosity. The gas-solid interface is assumed to have only one type of adsorption site. The adsorbed species on the interface and the vacant sites are then considered to form only one "phase" (in the sense of Kee *et al.* [34]). Note that in a more refined description, we could describe the existence of several types of adsorption sites; accordingly, the gas-solid interface would contain as many "phases" as the number of the different types of adsorption sites.

Therefore, the notion of "phase" as understood in [34] is not retained here, because it is redundant with the notion of domain. From now on, the term *phase* is understood in the sense of the multiphase-flow community: it can refer to one of the two volume domains, that is the gas or the solid phase. These two phases will be noted $\left(\mathcal{P}^{(m)}\right)_{m\in\{1,2\}}$, with the index $m = 1$ corresponding to the gas phase and $m = 2$ corresponding to the solid phase. The sharp interface between the two phases is noted Σ. As a convention, we suppose the following set of relations:

$$\begin{cases} \mathcal{P}^{(1)} \cap \Sigma = \emptyset \\ \mathcal{P}^{(2)} \cap \Sigma = \emptyset \\ \mathcal{P}^{(1)} \cup \mathcal{P}^{(2)} \cup \Sigma = \mathbb{R}^3. \end{cases} \tag{2.1}$$

To track the phases, we define *phase-indicator functions* $\chi^{(m)}$ such that for $m \in \{1, 2\}$:

$$\forall \mathbf{x} \in \mathbb{R}^3,\ \forall t \in \mathbb{R}^+, \quad \chi^{(m)}(\mathbf{x}, t) = \begin{cases} 1 & \text{if } \mathbf{x} \in \mathcal{P}^{(m)} \text{ at the instant } t \\ 0 & \text{otherwise.} \end{cases} \tag{2.2}$$

It is straightforward to show that:

$$\chi^{(1)}\chi^{(2)} = 0 \tag{2.3}$$

and $\forall m \in \{1, 2\},\ \forall n \in \mathbb{N}^*$,

$$\left(\chi^{(m)}\right)^n = \chi^{(m)}. \tag{2.4}$$

Unit normal vectors to the interface Σ, noted as $\hat{\mathbf{n}}^{(m)}$, are conventionally defined as oriented outwards from the phase $\mathcal{P}^{(m)}$. The partial derivatives of the phase-indicator functions $\chi^{(m)}$ then verify in the sense of distributions (see Appendix A):

$$\begin{cases} \boldsymbol{\nabla}\chi^{(m)} = -\hat{\mathbf{n}}^{(m)}\delta_\Sigma \\ \dfrac{\partial\chi^{(m)}}{\partial t} = \hat{\mathbf{w}} \cdot \hat{\mathbf{n}}^{(m)}\delta_\Sigma \end{cases} \tag{2.5}$$

where δ_Σ is the surface Dirac distribution associated with the interface Σ and $\hat{\mathbf{w}}$ is the velocity of the interface (formalized later).

2.3. Volume and surface fields

2.3.1. Volume fields

We first introduce *single-phase fields*, that describe local and instantaneous physical quantities in only one of the separate phases $\mathcal{P}^{(m)}$. For $m \in \{1, 2\}$, a single-phase field is noted in a generic way $\phi^{(m)}$. It is only

defined for $\mathbf{x} \in \mathcal{P}^{(m)}$. It is also supposed to be regular and bounded in space throughout $\mathcal{P}^{(m)}$, and in time as well.

From the couple of generic single-phase fields $\left(\phi^{(1)}, \phi^{(2)}\right)$, we can then build a *two-phase field* ϕ defined in all the space $\mathbb{R}^3$, and coinciding for $m \in \{1,2\}$ with $\phi^{(m)}$ in the phase $\mathcal{P}^{(m)}$. Mathematically, ϕ can be expressed as follows:

$$\phi = \sum_{m=1}^{2} \chi^{(m)} \phi^{(m)}. \tag{2.6}$$

Due to the regularity and boundedness assumptions for the single-phase fields $\phi^{(m)}$ in their associated phase m, sided limits at the interface Σ can thus be defined for all instant t:

$$\forall m \in \{1,2\},\ \forall \mathbf{x}_\Sigma \in \Sigma, \quad \begin{cases} \phi^{(m)}(\mathbf{x}_\Sigma, t) = \lim\limits_{\substack{\mathbf{x} \to \mathbf{x}_\Sigma \\ \mathbf{x} \in \mathcal{P}^{(m)}}} \left[\phi^{(m)}(\mathbf{x}, t)\right] = \lim\limits_{\substack{\mathbf{x} \to \mathbf{x}_\Sigma \\ \mathbf{x} \in \mathcal{P}^{(m)}}} \left[\phi(\mathbf{x}, t)\right]. \\ \boldsymbol{\nabla}\phi^{(m)}(\mathbf{x}_\Sigma, t) = \lim\limits_{\substack{\mathbf{x} \to \mathbf{x}_\Sigma \\ \mathbf{x} \in \mathcal{P}^{(m)}}} \left[\boldsymbol{\nabla}\phi^{(m)}(\mathbf{x}, t)\right] = \lim\limits_{\substack{\mathbf{x} \to \mathbf{x}_\Sigma \\ \mathbf{x} \in \mathcal{P}^{(m)}}} \left[\sum_{m=1}^{2} \chi^{(m)} \boldsymbol{\nabla}\phi^{(m)}\right]. \end{cases} \tag{2.7}$$

If the sided limits (2.7) differ at Σ, ϕ (respectively $\sum_{m=1}^{2} \chi^{(m)} \boldsymbol{\nabla}\phi^{(m)}$) has a jump discontinuity across Σ. If the sided limits (2.7) coincide at Σ, ϕ (respectively $\sum_{m=1}^{2} \chi^{(m)} \boldsymbol{\nabla}\phi^{(m)}$) has at most a removable discontinuity at Σ [1]. In this last situation, ϕ (respectively $\sum_{m=1}^{2} \chi^{(m)} \boldsymbol{\nabla}\phi^{(m)}$) will be termed as being continuous at the interface Σ, despite the formal discontinuity.

Finally, according to the definition (2.6), and equations (2.3) and (2.4), we have for any couple of two-phase fields ϕ and θ:

$$\sum_{m=1}^{2} \chi^{(m)} \phi^{(m)} \theta^{(m)} = \left(\sum_{m=1}^{2} \chi^{(m)} \phi^{(m)}\right) \left(\sum_{m=1}^{2} \chi^{(m)} \theta^{(m)}\right) = \phi\theta. \tag{2.8}$$

The relation (2.8) can be generalized to the product of an arbitrary number of two-phase variables.

2.3.2. Surface fields

Due to adsorption/recombination/desorption of species, the gas-solid interface possesses physical properties, which evolution is coupled to the dynamic of the gas and the solid phase. *Surface fields* [2]have therefore to be defined to describe the local and instantaneous physical properties of the interface Σ. These surface fields will be generically noted $\hat{\phi}$.

The velocity of the interface is an example of surface field. It can be decomposed into a normal and a tangential contribution:

$$\hat{\mathbf{w}} = \hat{\mathbf{w}}_\mathrm{n} + \hat{\mathbf{w}}_\mathrm{t}, \quad \text{with} \quad \hat{\mathbf{w}}_\mathrm{n} = \left(\hat{\mathbf{w}} \cdot \hat{\mathbf{n}}\right) \hat{\mathbf{n}}. \tag{2.9}$$

As Delhaye [19], we assume the following continuity equation at the interface:

$$\hat{\mathbf{w}}_\mathrm{t} = \mathbf{u}^{(1)} - \left(\mathbf{u}^{(1)} \cdot \hat{\mathbf{n}}^{(1)}\right) \hat{\mathbf{n}}^{(1)} = \mathbf{u}^{(2)} - \left(\mathbf{u}^{(2)} \cdot \hat{\mathbf{n}}^{(2)}\right) \hat{\mathbf{n}}^{(2)} \text{ at the interface } \Sigma. \tag{2.10}$$

Eq. (2.10), as well as continuity of temperature at the interface, can be demonstrated by assuming the production of entropy to be zero at the interface Σ [28].

[1] Indeed, as a consequence of Eq. (2.1) and Eq. (2.2), ϕ is null on the interface Σ; this value is unimportant, because Σ is a negligible subset of $\mathbb{R}^3$.

[2] In this work, what we call surface field has another meaning than the classic definition by Aris [4], especially concerning surface vector fields. In [4], a surface vector field is necessarily tangent to the surface, whereas it is not in the present work.

2.4. Taxonomy of species

The chemical composition in the volume domains (gas and solid phases) is described in terms of *mass fractions*. The single-phase mass fraction of a species k in the phase m is noted $Y_k^{(m)}$. At the interface Σ, the chemical composition is rather described in terms of *site fractions*. The site fraction of a species k is noted $\hat{Z}_k$ and corresponds to the local fraction of surface sites occupied by the species k. Its relation with the mass of the species k per unit surface will be detailed in Sec. 3.2.

Moreover, the conventions established in [34] are followed here. The total number of chemical species is noted K, and each species $k \in [\![1, K]\!]$ is relative to a domain (gas, solid or interface). This formalism then defines three distinct types of species for our problem. They are listed below.

- *Gas species*: corresponding to species that compose the gas phase. Their set of indices k is noted $\Omega^{(1)}$. Their mass fractions, diffusion velocity and mass reaction rate verify the conditions:

$$\begin{cases} \displaystyle\sum_{k\in\Omega^{(1)}} Y_k^{(1)} = 1 \\ \displaystyle\sum_{k\in\Omega^{(1)}} Y_k^{(1)}\mathbf{V}_k^{(1)} = 0 \\ \displaystyle\sum_{k\in\Omega^{(1)}} \dot{\omega}_k^{(1)} = 0 \end{cases} \tag{2.11}$$

  Although these species are not present in the solid phase $\mathcal{P}^{(2)}$ and at the gas-solid interface Σ, we define a mass fraction in the solid phase $\mathcal{P}^{(2)}$ and a site fraction at the interface Σ for the gas species that are equal to zero:

$$\forall k \in \Omega^{(1)}, \quad \begin{cases} Y_k^{(2)} = 0 \text{ in the solid phase } \mathcal{P}^{(2)} \\ \hat{Z}_k = 0 \text{ at the interface } \Sigma. \end{cases} \tag{2.12}$$

- *Solid species*: corresponding to species forming the solid phase. Their set of indices is noted $\Omega^{(2)}$. In our problem their chemical composition does not change with time. Therefore, the description of the chemical composition in the solid can be reduced to one effective species k_s. The associated conditions thus writes:

$$\begin{cases} \displaystyle\sum_{k\in\Omega^{(2)}} Y_k^{(2)} = Y_{k_s}^{(2)} = 1 \\ \displaystyle\sum_{k\in\Omega^{(2)}} Y_k^{(2)}\mathbf{V}_k^{(2)} = \mathbf{V}_{k_s}^{(2)} = 0 \text{ in the solid phase } \mathcal{P}^{(2)}. \\ \displaystyle\sum_{k\in\Omega^{(2)}} \dot{\omega}_k^{(2)} = \dot{\omega}_{k_s}^{(2)} = 0 \end{cases} \tag{2.13}$$

  Although species k_s is not present in the gas phase $\mathcal{P}^{(1)}$ and at the gas-solid interface Σ, we define a mass fraction in the gas phase $\mathcal{P}^{(1)}$ and a site fraction at the interface Σ for the species k_s that are equal to zero:

$$\begin{cases} Y_{k_s}^{(1)} = 0 \text{ in the gas phase } \mathcal{P}^{(1)} \\ \hat{Z}_{k_s} = 0 \text{ at the interface } \Sigma. \end{cases} \tag{2.14}$$

- *Surface species*: corresponding to species adsorbed on the surface of the solid particles. Their set of indices is noted $\Omega^{(\Sigma)}$. The normalization condition for these surface species writes:

$$\hat{Z}_* + \sum_{k\in\Omega^{(\Sigma)}} \hat{Z}_k = 1 \text{ at the interface } \Sigma \tag{2.15}$$

  with $\hat{Z}_*$ the fraction of vacant sites.

Although the surface species are not present in the solid and gas phases, we define a mass fraction there, equal to zero:

$$\forall k \in \Omega^{(\Sigma)}, \begin{cases} Y_k^{(1)} = 0 \text{ in the gas phase } \mathcal{P}^{(1)} \\ Y_k^{(2)} = 0 \text{ in the solid phase } \mathcal{P}^{(2)}. \end{cases} \tag{2.16}$$

We can then demonstrate the global normalization condition for the two-phase mass fractions::

$$\sum_{k=1}^{K} Y_k = 1 \text{ almost everywhere.} \tag{2.17}$$

Indeed, this equation does not hold on Σ because $\forall k \in [\![1, K]\!]$, Y_k is null at the interface with our conventions.

2.5. Surface reactions

The formal description of homogeneous reactions can be found in [45] and is not reported here. In this section, an analogous description is carried out for surface reactions.

While homogeneous reactions only involve gas species, surface reactions can involve gas, solid, and interface species. But since we assumed that the solid particles are partially inert, surface reactions do not involve solid species in our problem. Also, the *open-site convention* is adopted in this study to describe adsorption/recombination/desorption processes [34].

We assume the existence of M_Σ surface reactions. A particular surface reaction $j \in [\![1, M_\Sigma]\!]$ can be described in this formalism by the general balance chemical relation:

$$\sum_{k \in \Omega^{(1)} \cup \Omega^{(\Sigma)}} \nu'_{kj} \mathcal{M}_k + \nu'_{*j} \mathcal{M}_* \leftrightarrows \sum_{k \in \Omega^{(1)} \cup \Omega^{(\Sigma)}} \nu''_{kj} \mathcal{M}_k + \nu''_{*j} \mathcal{M}_* \tag{2.18}$$

where, $\mathcal{M}_k$ represents a molecule of species k, and $\mathcal{M}_*$ a vacant surface site. The quantities ν'_{kj} and ν''_{kj} are the stoichiometric coefficients of species k in reaction j for reactants and products respectively, while ν'_{*j} and ν''_{*j} are the counterparts of ν'_{kj} and ν''_{kj} for vacant surface sites. The sum is taken on gas and surface species, $k \in \Omega^{(1)} \cup \Omega^{(\Sigma)}$.

Eq. (2.18) can describe any type of surface reaction relevant to our problem, namely adsorption, recombination, and desorption. Here is an example of surface reactions from [2], where catalytic combustion of hydrogen on a platinum surface is numerically studied:

- the adsorption from the gas phase (1) of the gas radical H on the surface Σ:

$$H_{(1)} + \mathcal{M}_* \rightarrow H_{(\Sigma)} \tag{2.19}$$

- the recombination of two adsorbed radicals at the surface, immediately followed by the desorption of the resulting molecule into the gas phase:

$$2H_{(\Sigma)} \rightarrow H_{2(1)} + 2\mathcal{M}_* \tag{2.20}$$

As for homogeneous reactions, surface reactions conserve mass. Introducing the molar mass W_k of species k, this conservation principle writes for all surface reactions $j \in [\![1, M_\Sigma]\!]$:

$$\sum_{k \in \Omega^{(1)} \cup \Omega^{(\Sigma)}} \left(\nu''_{kj} - \nu'_{kj}\right) W_k = 0. \tag{2.21}$$

If the rate-of-progress of these surface reactions is noted $\hat{\mathcal{Q}}_j$, the net molar reaction rate of species k by the surface reaction j per unit surface is then expressed as:

$$\dot{\hat{s}}_{kj} = \left(\nu''_{kj} - \nu'_{kj}\right) \hat{\mathcal{Q}}_j \tag{2.22}$$

and the molar reaction rate of species k by all M_Σ surface reactions per unit surface is thus

$$\dot{\hat{s}}_k = \sum_{j=1}^{M_\Sigma} \dot{\hat{s}}_{kj}. \tag{2.23}$$

Using Eqs. (2.23) and (2.21) leads to

$$\sum_{k\in\Omega^{(1)}\cup\Omega^{(\Sigma)}} W_k \dot{\hat{s}}_k = \sum_{j=1}^{M_\Sigma} \left(\sum_{k\in\Omega^{(1)}\cup\Omega^{(\Sigma)}} \left(\nu''_{kj} - \nu'_{kj}\right) W_k \right) \hat{\mathcal{Q}}_j = 0 \tag{2.24}$$

which shows that the total mass is conserved during the surface reactions.

As the density of surface sites is assumed to be constant in the present article, surface sites should be conserved by each surface reaction. According to [34], a parameter σ_k is introduced to account for the fact that a large molecule can occupy several surface sites. The integer σ_k is called *site occupancy number*; it is the number of sites that a molecule of species k occupies when it is adsorbed on the surface. It is considered a property of the species k on the considered surface. Therefore, assuming that a molecule of a surface species $k \in \Omega^{(\Sigma)}$ occupies σ_k sites, the surface reaction $j \in [\![1, M_\Sigma]\!]$ (2.18) should verify:

$$\left(\sum_{k\in\Omega^{(\Sigma)}} \left(\nu''_{kj} - \nu'_{kj}\right) \sigma_k \right) + \left(\nu''_{*j} - \nu'_{*j}\right) = 0. \tag{2.25}$$

Coming back to the surface reactions described by Eqs (2.19) and (2.20), the site occupancy number of $H_{(\Sigma)}$ is $\sigma_{H_{(\Sigma)}} = 1$. It is straightforward to verify that these two reactions verify Eq. (2.25).

Regarding more general descriptions, if the assumption of constant site density is relaxed, then each surface reaction does not necessarily verify Eq. (2.25); see [34] to see how such situation can be described.

3. Two-field representation

In this section, the *two-field representation* of the gas-solid flow is derived. For each physical variable describing the flow, this representation consists in: i) two *local and instantaneous single-phase equations*, each one being associated with one of the two phases and solely valid in it; ii) a *local and instantaneous jump condition* at the interface, acting as a boundary condition for the considered variable.

First, the integral-balance method [19] is outlined in Sec. 3.1. Then, this approach is applied to the conservation of mass (Sec. 3.2), momentum (Sec. 3.3), and energy (Sec. 3.4). The integral balances are written to obtain the same, well known, local and instantaneous reactive gas-phase equations as in [45]. The internal structure of the interface and the effects of surface reactions appear in the derived jump equations. Such jump equations are consistent with previously derived ones, for single-component [19, 28] and multi-component [49, 29] two-phase flow with a material interface. They are consistent with the formalism of the Surface Chemkin [13] or Cantera [25] software, which can be used to numerically compute physical quantities that are left unmodeled in the present study. Precisions on this matter are provided in the last part of this section (Sec. 3.5).

3.1. General approach

The two-field representation can be obtained by systematically applying conservation principles to a material volume V that is spread over the two phases (see Fig. 1). The following notations are adopted:

- $V^{(m)} = V \cap \mathcal{P}^{(m)}$ is the part of the volume V containing the phase $\mathcal{P}^{(m)}$.
- $\mathcal{S} = \Sigma \cap V$ is the portion of the interface Σ contained in the volume V.
- $(\partial V)^{(m)} = \partial V \cap V^{(m)}$ is the portion of the surface ∂V delimiting the volume V that is included in $V^{(m)}$.

- $\partial\left(V^{(m)}\right) = (\partial V)^{(m)} \cup \mathcal{S}$ is the closed surface that surrounds the volume $V^{(m)}$.
- $\mathbf{n}^{(m)}$ is the normal vector to $\partial\left(V^{(m)}\right)$ that is directed outward from $V^{(m)}$. On $\mathcal{S} = \Sigma \cap \partial\left(V^{(m)}\right)$, it coincides with the normal vector to Σ noted $\hat{\mathbf{n}}^{(m)}$ in Sec. 2.2.
- $\mathcal{C} = \partial\mathcal{S}$ is the closed contour that circles the surface $\mathcal{S}$. We also have the relation $\mathcal{C} = \partial V \cap \Sigma$.
- $\hat{\mathbf{N}}$ is the vector that is normal to $\mathcal{C}$, tangent to Σ, and directed outwards from $\mathcal{S}$.

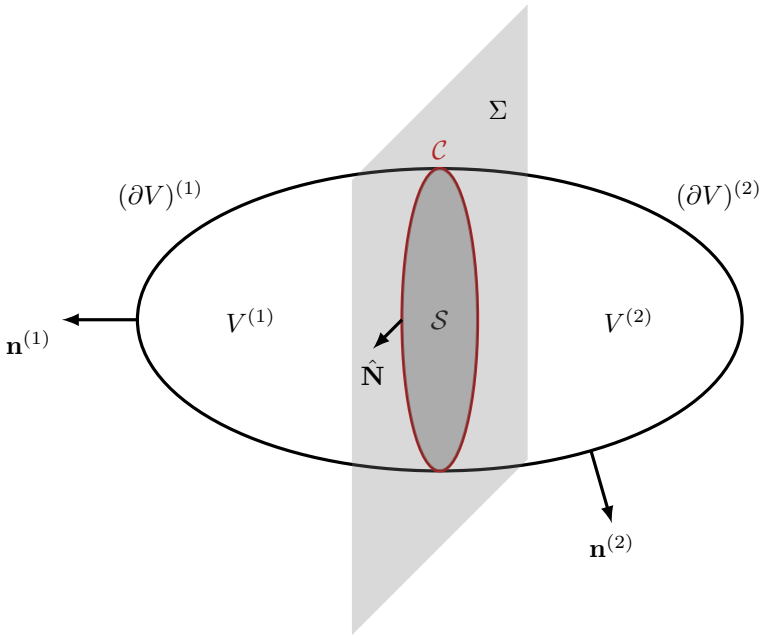

Figure 1: The material volume $V = V^{(1)} \cup V^{(2)}$ used to apply conservation principles.

Any conservation principle applied to the material volume V can be put in the general form:

$$\frac{\mathrm{d}}{\mathrm{d}t}\left(\sum_{m=1}^{2}\int_{V^{(m)}}\phi^{(m)}\mathrm{d}^3V + \int_{\mathcal{S}}\hat{\phi}\mathrm{d}^2S\right) = \begin{cases} -\sum_{m=1}^{2}\left[\int_{(\partial V)^{(m)}}\mathbf{J}^{(m)}\cdot\mathbf{n}^{(m)}\mathrm{d}^2S\right] \\ -\oint_{\mathcal{C}}\hat{\mathbf{J}}\cdot\hat{\mathbf{N}}\mathrm{d}l \\ +\sum_{m=1}^{2}\left[\int_{V^{(m)}}\Theta^{(m)}\mathrm{d}^3V\right] \\ +\int_{\mathcal{S}}\hat{\Theta}\mathrm{d}^2S \end{cases} \tag{3.1}$$

where

- for $m \in \{1,2\}$, $\phi^{(m)}$ is the conserved quantity per unit volume in the phase $\mathcal{P}^{(m)}$;
- $\hat{\phi}$ is the conserved quantity per unit surface at the interface Σ;
- for $m \in \{1,2\}$, $\mathbf{J}^{(m)}$ is a generic diffusion flux in the phase $\mathcal{P}^{(m)}$;
- $\hat{\mathbf{J}}$ is a generic diffusion flux at the interface Σ. This vector is tangent to Σ;
- for $m \in \{1,2\}$, $\Theta^{(m)}$ is a generic volume source term in the phase $\mathcal{P}^{(m)}$.

- $\hat{\Theta}$ is a generic surface source term.

From the fundamental equation (3.1), the application of mathematical transformations enables to find the corresponding local equations in each separate phase $m \in \{1, 2\}$ and the local jump equation at the interface Σ.

- **Total derivative term**: the application of the Reynolds transport theorem (see Appendix C and Theorem 2) yields

$$\begin{aligned}
\frac{\mathrm{d}}{\mathrm{d}t}\int_{V^{(m)}} \phi^{(m)}\mathrm{d}^3V &= \int_{V^{(m)}} \frac{\partial \phi^{(m)}}{\partial t}\mathrm{d}^3V + \int_{(\partial V)^{(m)}} \phi^{(m)}\mathbf{u}^{(m)}\cdot\mathbf{n}^{(m)}\mathrm{d}^2S + \int_{\mathcal{S}} \phi^{(m)}\hat{\mathbf{w}}\cdot\hat{\mathbf{n}}^{(m)}\mathrm{d}^2S \\
&= \begin{cases} & \displaystyle\int_{V^{(m)}} \frac{\partial \phi^{(m)}}{\partial t}\mathrm{d}^3V \\ + & \displaystyle\int_{(\partial V)^{(m)}} \phi^{(m)}\mathbf{u}^{(m)}\cdot\mathbf{n}^{(m)}\mathrm{d}^2S \\ + & \displaystyle\int_{\mathcal{S}} \left[\phi^{(m)}\hat{\mathbf{w}}\cdot\hat{\mathbf{n}}^{(m)} + \phi^{(m)}\mathbf{u}^{(m)}\cdot\hat{\mathbf{n}}^{(m)} - \phi^{(m)}\mathbf{u}^{(m)}\cdot\hat{\mathbf{n}}^{(m)}\right]\mathrm{d}^2S \end{cases} \\
&= \int_{V^{(m)}} \frac{\partial \phi^{(m)}}{\partial t}\mathrm{d}^3V + \oint_{\partial\left(V^{(m)}\right)} \phi^{(m)}\mathbf{u}^{(m)}\cdot\mathbf{n}^{(m)}\mathrm{d}^2S + \int_{\mathcal{S}} \phi^{(m)}\left(\hat{\mathbf{w}} - \mathbf{u}^{(m)}\right)\cdot\hat{\mathbf{n}}^{(m)}\mathrm{d}^2S
\end{aligned}$$

  so that

$$\frac{\mathrm{d}}{\mathrm{d}t}\int_{V^{(m)}} \phi^{(m)}\mathrm{d}^3V = \int_{V^{(m)}} \left[\frac{\partial \phi^{(m)}}{\partial t} + \boldsymbol{\nabla}\cdot\left(\phi^{(m)}\mathbf{u}^{(m)}\right)\right]\mathrm{d}^3V - \int_{\mathcal{S}} \phi^{(m)}\left(\mathbf{u}^{(m)} - \hat{\mathbf{w}}\right)\cdot\hat{\mathbf{n}}^{(m)}\mathrm{d}^2S. \quad (3.2)$$

  The application of the transport theorem for Surface (see Appendix C and Theorem 3) provides

$$\frac{\mathrm{d}}{\mathrm{d}t}\left(\int_{\mathcal{S}} \hat{\phi}\mathrm{d}^2S\right) = \int_{\mathcal{S}} \left(\frac{\mathrm{d}\hat{\phi}}{\mathrm{d}t} + \hat{\phi}\boldsymbol{\nabla}_\Sigma\cdot\hat{\mathbf{w}}\right)\mathrm{d}^2S. \quad (3.3)$$

- **Flux term term in volume**:

$$\int_{(\partial V)^{(m)}} \mathbf{J}^{(m)}\cdot\mathbf{n}^{(m)}\mathrm{d}^2S = \oint_{\partial\left(V^{(m)}\right)} \mathbf{J}^{(m)}\cdot\mathbf{n}^{(m)}\mathrm{d}^2S - \int_{\mathcal{S}} \mathbf{J}^{(m)}\cdot\hat{\mathbf{n}}^{(m)}\mathrm{d}^2S$$

  such that

$$\int_{(\partial V)^{(m)}} \mathbf{J}^{(m)}\cdot\mathbf{n}^{(m)}\mathrm{d}^2S = \int_{V^{(m)}} \boldsymbol{\nabla}\cdot\mathbf{J}^{(m)}\mathrm{d}^3V - \int_{\mathcal{S}} \mathbf{J}^{(m)}\cdot\hat{\mathbf{n}}^{(m)}\mathrm{d}^2S. \quad (3.4)$$

- **Flux term on the surface**: The application of the Gauss theorem for surface (see Appendix C and Theorem 4) gives

$$\oint_{\mathcal{C}} \hat{\mathbf{J}}\cdot\hat{\mathbf{N}}\mathrm{d}l = \int_{\mathcal{S}} \boldsymbol{\nabla}_\Sigma\cdot\hat{\mathbf{J}}\mathrm{d}^2S. \quad (3.5)$$

By substituting Eqs. (3.2),(3.3),(3.4),(3.5) into Eq. (3.1), we obtain:

$$0 = \begin{cases} & \displaystyle\sum_{m=1}^{2}\int_{V^{(m)}} \left\{\frac{\partial \phi^{(m)}}{\partial t} + \boldsymbol{\nabla}\cdot\left(\phi^{(m)}\mathbf{u}^{(m)}\right) - \left(-\boldsymbol{\nabla}\cdot\mathbf{J}^{(m)} + \Theta^{(m)}\right)\right\}\mathrm{d}^3V \\ - & \displaystyle\int_{\mathcal{S}} \left\{\sum_{m=1}^{2}\left[\phi^{(m)}\left(\mathbf{u}^{(m)} - \hat{\mathbf{w}}\right) + \mathbf{J}^{(m)}\right]\cdot\hat{\mathbf{n}}^{(m)} - \left(\frac{\mathrm{d}\hat{\phi}}{\mathrm{d}t} + \hat{\phi}\boldsymbol{\nabla}_\Sigma\cdot\hat{\mathbf{w}} + \boldsymbol{\nabla}_\Sigma\cdot\hat{\mathbf{J}} - \hat{\Theta}\right)\right\}\mathrm{d}^2S. \end{cases} \quad (3.6)$$

Since Eq. (3.6) has been obtained for any material volume V cut by the interface Σ (any $V^{(m)}$, any $\mathcal{S}$), the development finally leads to

- the local single-phase equation for each $m \in \{1,2\}$

$$\frac{\partial \phi^{(m)}}{\partial t} + \boldsymbol{\nabla} \cdot \left(\phi^{(m)} \mathbf{u}^{(m)} \right) = -\boldsymbol{\nabla} \cdot \mathbf{J}^{(m)} + \Theta^{(m)} \quad \text{in the phase } \mathcal{P}^{(m)}; \tag{3.7}$$

- the jump equation

$$\sum_{m=1}^{2} \left[\phi^{(m)} \left(\mathbf{u}^{(m)} - \hat{\mathbf{w}} \right) + \mathbf{J}^{(m)} \right] \cdot \hat{\mathbf{n}}^{(m)} = \frac{\mathrm{d}\hat{\phi}}{\mathrm{d}t} + \hat{\phi} \boldsymbol{\nabla}_\Sigma \cdot \hat{\mathbf{w}} + \boldsymbol{\nabla}_\Sigma \cdot \hat{\mathbf{J}} - \hat{\Theta} \quad \text{at the interface } \Sigma. \tag{3.8}$$

  Since the solid phase is not consumed by any heterogeneous process, the interface velocity $\hat{\mathbf{w}}$ and the velocity field $\mathbf{u}^{(2)}$ coincide at Σ. This statement is rigorously demonstrated in Eq. (3.19). In this case, the general jump equation (3.8) can take the simplified form

$$\phi^{(1)} \left(\mathbf{u}^{(1)} - \hat{\mathbf{w}} \right) \cdot \hat{\mathbf{n}}^{(1)} + \sum_{m=1}^{2} \mathbf{J}^{(m)} \cdot \hat{\mathbf{n}}^{(m)} = \frac{\mathrm{d}\hat{\phi}}{\mathrm{d}t} + \boldsymbol{\nabla}_\Sigma \cdot \hat{\mathbf{J}} - \hat{\Theta} \quad \text{at the interface } \Sigma. \tag{3.9}$$

3.2. Species and mass

Let $k \in [\![1, K]\!]$, where K is the total number of chemical species in the overall system (including all the domains). We apply the conservation principle (3.1) using the following quantities:

- $\phi^{(m)} = \rho^{(m)} Y_k^{(m)}$ the mass of the species k per unit volume in the phase $\mathcal{P}^{(m)}$, for $m \in \{1,2\}$;
- $\hat{\phi} = \frac{W_k}{\sigma_k} \hat{\Gamma} \hat{Z}_k$ the mass of the species k per unit surface on the interface Σ, with $\hat{\Gamma}$ *the density of surface sites* at Σ, and σ_k the *site occupancy number* (cf. Sec. 2.5). According to the assumptions enunciated in Sec. 2.1, the density of surface sites $\hat{\Gamma}$ is a constant, characterizing the considered surface. To lighten the notation we write

$$\hat{\rho}_k = \frac{W_k}{\sigma_k} \hat{\Gamma} \hat{Z}_k; \tag{3.10}$$

- $\mathbf{J}^{(m)} = \rho^{(m)} Y_k^{(m)} \mathbf{V}_k^{(m)}$ the diffusion flux of the species k in the phase $\mathcal{P}^{(m)}$, for $m \in \{1,2\}$;
- $\hat{\mathbf{J}} = \mathbf{0}$ (no surface diffusion of species);
- $\Theta^{(m)} = \dot{\omega}_k^{(m)}$ the mass reaction rate of the species k per unit volume due to homogeneous reactions in the phase $\mathcal{P}^{(m)}$. It is zero in the solid phase;
- $\hat{\Theta} = W_k \dot{\hat{s}}_k$ the mass reaction rate of species k per unit surface due to surface reactions at the interface Σ.

From Eq. (3.7), we deduce the general local species equation in each phase $m \in \{1,2\}$ [45]:

$$\forall k \in [\![1, K]\!], \quad \frac{\partial}{\partial t} \left(\rho^{(m)} Y_k^{(m)} \right) + \boldsymbol{\nabla} \cdot \left[\rho^{(m)} Y_k^{(m)} \left(\mathbf{u}^{(m)} + \mathbf{V}_k^{(m)} \right) \right] = \dot{\omega}_k^{(m)} \quad \text{in the phase } \mathcal{P}^{(m)}. \tag{3.11}$$

According to Eq. (3.9), the solution of these local equations shall satisfy the following jump condition:

$$\forall k \in [\![1, K]\!], \quad \rho^{(1)} Y_k^{(1)} \left(\mathbf{u}^{(1)} - \hat{\mathbf{w}} \right) \cdot \hat{\mathbf{n}}^{(1)} + \sum_{m=1}^{2} \rho^{(m)} Y_k^{(m)} \mathbf{V}_k^{(m)} \cdot \hat{\mathbf{n}}^{(m)} = \frac{\mathrm{d}\hat{\rho}_k}{\mathrm{d}t} - W_k \dot{\hat{s}}_k \quad \text{at the interface } \Sigma. \tag{3.12}$$

Eq. (3.12) being written for any type of species, we consider the special cases of gas, solid, and surface species in the following paragraphs.

3.2.1. Gas species

The special case of a gas species $k \in \Omega^{(1)}$ is considered. Such a species is absent from the solid phase and the interface, so that only the local equation in the gas phase $\mathcal{P}^{(1)}$ is of interest. According to Eq. (3.11) and Eq. (2.12), this equation writes [45]:

$$\forall k \in \Omega^{(1)}, \quad \frac{\partial}{\partial t}\left(\rho^{(1)} Y_k^{(1)}\right) + \boldsymbol{\nabla} \cdot \left[\rho^{(1)} Y_k^{(1)} \left(\mathbf{u}^{(1)} + \mathbf{V}_k^{(1)}\right)\right] = \dot{\omega}_k^{(1)} \text{ in the phase } \mathcal{P}^{(1)}. \tag{3.13}$$

According to Eq. (3.12) and Eq. (2.12) the jump equation for the gas species is then:

$$\forall k \in \Omega^{(1)}, \quad \rho^{(1)} Y_k^{(1)} \left(\mathbf{u}^{(1)} + \mathbf{V}_k^{(1)} - \hat{\mathbf{w}}\right) \cdot \hat{\mathbf{n}}^{(1)} = -W_k \dot{\hat{s}}_k \text{ at the interface } \Sigma. \tag{3.14}$$

If all equations (3.13) are summed over $k \in \Omega^{(1)}$ with the use of (2.11), the mass conservation writes:

$$\frac{\partial \rho^{(1)}}{\partial t} + \boldsymbol{\nabla} \cdot \left(\rho^{(1)} \mathbf{u}^{(1)}\right) = 0 \text{ in the phase gas } \mathcal{P}^{(1)}. \tag{3.15}$$

If all jump equations (3.14) are summed over $k \in \Omega^{(1)}$ with the use of (2.11), one can obtain the following condition at the interface:

$$\rho^{(1)} \left(\mathbf{u}^{(1)} - \hat{\mathbf{w}}\right) \cdot \hat{\mathbf{n}}^{(1)} = -\sum_{k \in \Omega^{(1)}} W_k \dot{\hat{s}}_k. \tag{3.16}$$

3.2.2. Solid species

The special case of the unique solid species k_s is considered. In this case, the application of Eq. (3.11) and (2.13) directly provides the local equation for mass conservation:

$$\frac{\partial \rho^{(2)}}{\partial t} + \boldsymbol{\nabla} \cdot \left(\rho^{(2)} \mathbf{u}^{(2)}\right) = 0 \text{ in the solid phase } \mathcal{P}^{(2)}. \tag{3.17}$$

To derive the corresponding condition at the interface, we have to use the general jump condition Eq. (3.8) instead of Eq. (3.9). Applying Eq. (3.8) to the particular case of the solid species k_s, together with (2.13) and Eq. (2.14), we obtain:

$$\rho^{(2)} \left(\mathbf{u}^{(2)} - \hat{\mathbf{w}}\right) \cdot \hat{\mathbf{n}}^{(2)} = -W_k \dot{\hat{s}}_{k_s} \quad \text{at the interface } \Sigma. \tag{3.18}$$

Since we assumed that the solid particles are not consumed by heterogeneous combustion, and that the surface reactions are written in the open-site convention, the mass reaction rate per unit surface $W_k \dot{\hat{s}}_{k_s}$ is zero, and Eq. (3.18) becomes

$$\left(\mathbf{u}^{(2)} - \hat{\mathbf{w}}\right) \cdot \hat{\mathbf{n}}^{(2)} = \mathbf{0} \quad \text{at the interface } \Sigma. \tag{3.19}$$

Eq. (3.19) has been used to simplify Eq. (3.8) into Eq. (3.9), and will be constantly used in this work. Note that this relation would not hold anymore for a solid particle consumed by heterogeneous combustion.

3.2.3. Surface species

The special case a surface species $k \in \Omega^{(\Sigma)}$ is considered. Such a species is only present at the interface Σ. Its description thus reduces to the surface equation (3.12), that writes together with Eq. (2.16)

$$\forall k \in \Omega^{(\Sigma)}, \quad \frac{\mathrm{d}\hat{\rho}_k}{\mathrm{d}t} = W_k \dot{\hat{s}}_k \quad \text{at the interface } \Sigma. \tag{3.20}$$

Using Eq. (3.10) and the assumption of constant density of surface sites $\hat{\Gamma}$, we can obtain the local equation for the site fractions:

$$\forall k \in \Omega^{(\Sigma)}, \quad \frac{\mathrm{d}\hat{Z}_k}{\mathrm{d}t} = \sigma_k \frac{\dot{\hat{s}}_k}{\hat{\Gamma}} \quad \text{at the interface } \Sigma. \tag{3.21}$$

If Eq. (3.20) is summed over $k \in \Omega^{(\Sigma)}$, one obtains the evolution equation for the total excess mass $\hat{\rho}$:

$$\frac{\mathrm{d}\hat{\rho}}{\mathrm{d}t} = \sum_{k\in\Omega^{(\Sigma)}} W_k \dot{\hat{s}}_k = -\sum_{k\in\Omega^{(1)}} W_k \dot{\hat{s}}_k. \tag{3.22}$$

The second equality in (3.22) is provided by Eq. (2.24).

3.3. Momentum

In this section, the conservation of momentum is written for the material volume V. The general balance equation (3.1) has been written for a scalar quantity. Here we extend its formulation for a physical quantity described by the single-phase vector fields $\left(\boldsymbol{\phi}^{(m)}\right)_{m\in\{1,2\}}$ and the surface vector field $\hat{\boldsymbol{\phi}}$:

$$\frac{\mathrm{d}}{\mathrm{d}t}\left(\sum_{m=1}^{2}\int_{V^{(m)}} \boldsymbol{\phi}^{(m)}\mathrm{d}^3V + \int_{\mathcal{S}} \hat{\boldsymbol{\phi}}\mathrm{d}^2S\right) = \begin{cases} -\displaystyle\sum_{m=1}^{2}\left[\int_{(\partial V)^{(m)}} \boldsymbol{J}^{(m)}\cdot\hat{\mathbf{n}}^{(m)}\mathrm{d}^2S\right] \\ -\displaystyle\oint_{\mathcal{C}} \hat{\boldsymbol{J}}\cdot\hat{\mathbf{N}}\mathrm{d}l \\ +\displaystyle\sum_{m=1}^{2}\left[\int_{V^{(m)}} \boldsymbol{\Theta}^{(m)}\mathrm{d}^3V\right] \\ +\displaystyle\int_{\mathcal{S}} \hat{\boldsymbol{\Theta}}\mathrm{d}^2S \end{cases} \tag{3.23}$$

where $\boldsymbol{J}^{(m)}$ are volume second-order tensor fields modeling diffusion fluxes in their respective phase, $\hat{\boldsymbol{J}}$ is a surface second-order tensor field, $\boldsymbol{\Theta}^{(m)}$ are volume vector fields modeling a volume source term, and $\hat{\boldsymbol{\Theta}}$ is a surface vector field modeling a surface source term.

For simplification purposes, we consider the special case where the surface tensor field $\hat{\boldsymbol{J}}$ is diagonal; therefore, there exists a surface scalar field $\hat{J}$ such that the contour integral in Eq. (3.23) writes:

$$\oint_{\mathcal{C}} \hat{\boldsymbol{J}}\cdot\hat{\mathbf{N}}\mathrm{d}l = \oint_{\mathcal{C}} \hat{J}\hat{\mathbf{N}}\mathrm{d}l \tag{3.24}$$

The same mathematical manipulation used for Eq. 3.1 can be applied to Eq. (3.23) (for each component), except for the integral on the contour $\mathcal{C}$ (3.24), that is transformed using Eq. (C.4). This provides generic local equations for $m \in \{1,2\}$:

$$\frac{\partial\boldsymbol{\phi}^{(m)}}{\partial t} + \boldsymbol{\nabla}\cdot\left(\boldsymbol{\phi}^{(m)}\mathbf{u}^{(m)}\right) = -\boldsymbol{\nabla}\cdot\boldsymbol{J}^{(m)} + \boldsymbol{\Theta}^{(m)} \quad \text{in the phase } \mathcal{P}^{(m)} \tag{3.25}$$

and a generic jump equation:

$$\boldsymbol{\phi}^{(1)}\left[\left(\mathbf{u}^{(1)}-\hat{\mathbf{w}}\right)\cdot\hat{\mathbf{n}}^{(1)}\right] + \sum_{m=1}^{2}\boldsymbol{J}^{(m)}\cdot\hat{\mathbf{n}}^{(m)} = \frac{\mathrm{d}\hat{\boldsymbol{\phi}}}{\mathrm{d}t} + \boldsymbol{\nabla}_\Sigma\hat{J} - \left(\boldsymbol{\nabla}_\Sigma\cdot\hat{\mathbf{n}}\right)\hat{J}\hat{\mathbf{n}} - \hat{\boldsymbol{\Theta}} \quad \text{at the interface } \Sigma, \tag{3.26}$$

where $\boldsymbol{\nabla}_\Sigma\hat{J}$ designates the surface gradient of the scalar surface field $\hat{J}$. We apply the balance (3.23) using the following quantities:

- $\boldsymbol{\phi}^{(m)} = \rho^{(m)}\mathbf{u}^{(m)}$ the momentum per unit volume in the phase $\mathcal{P}^{(m)}$, for $m \in \{1,2\}$;
- $\hat{\boldsymbol{\phi}} = \hat{\rho}\hat{\mathbf{w}}$ the momentum per unit surface at the interface Σ;
- $\boldsymbol{J}^{(m)} = -\boldsymbol{\sigma}^{(m)}$, with $\boldsymbol{\sigma}^{(m)}$ the stress tensor in the phase $\mathcal{P}^{(m)}$, for $m \in \{1,2\}$. It is assumed to have the form:

$$\boldsymbol{\sigma}^{(m)} = -P^{(m)}\mathbf{I} + \mu^{(m)}\left(\boldsymbol{\nabla}\mathbf{u}^{(m)} + \boldsymbol{\nabla}^\top\mathbf{u}^{(m)} - \frac{2}{3}\left(\boldsymbol{\nabla}\cdot\mathbf{u}^{(m)}\right)\mathbf{I}\right) + \kappa^{(m)}\left(\boldsymbol{\nabla}\cdot\mathbf{u}^{(m)}\right)\mathbf{I} \tag{3.27}$$

where $P^{(m)}$, $\mu^{(m)}$ and $\kappa^{(m)}$ are respectively the pressure, the shear viscosity and the bulk viscosity in the phase $\mathcal{P}^{(m)}$. According to our assumptions, the shear viscosity in the solid phase $\mathcal{P}^{(2)}$ verifies

$$\mu^{(2)} \to \infty \tag{3.28}$$

that has for consequence to enforce a rigid-body motion in the solid phase:

$$\boldsymbol{\nabla}\mathbf{u}^{(2)} + \boldsymbol{\nabla}^{\top}\mathbf{u}^{(2)} = \mathbf{0} \quad \text{in the solid phase } \mathcal{P}^{(2)}; \tag{3.29}$$

- $\hat{J} = 0$ (no surface tension effects);
- $\boldsymbol{\Theta}^{(m)} = \rho^{(m)}\mathbf{g}$ the weight force per unit volume exerted on the phase $\mathcal{P}^{(m)}$,
- $\hat{\boldsymbol{\Theta}} = \hat{\rho}\mathbf{g}$ the weight force per unit surface exerted on the interface Σ.

From Eq. (3.25), we deduce the local equations in each phase $m \in \{1, 2\}$ [45]:

$$\frac{\partial}{\partial t}\left(\rho^{(m)}\mathbf{u}^{(m)}\right) + \boldsymbol{\nabla}\cdot\left(\rho^{(m)}\mathbf{u}^{(m)}\mathbf{u}^{(m)}\right) = \boldsymbol{\nabla}\cdot\boldsymbol{\sigma}^{(m)} + \rho^{(m)}\mathbf{g} \quad \text{in the phase } \mathcal{P}^{(m)}. \tag{3.30}$$

According to Eq. (3.26), the solution of these local equations shall satisfy the following jump condition:

$$\rho^{(1)}\mathbf{u}^{(1)}\left[\left(\mathbf{u}^{(1)} - \hat{\mathbf{w}}\right)\cdot\hat{\mathbf{n}}^{(1)}\right] - \sum_{m=1}^{2}\boldsymbol{\sigma}^{(m)}\cdot\hat{\mathbf{n}}^{(m)} = \frac{\mathrm{d}}{\mathrm{d}t}\left(\hat{\rho}\hat{\mathbf{w}}\right) - \hat{\rho}\mathbf{g}. \tag{3.31}$$

The dynamical effects due to the mass of the interface are considered to be negligible, so the retained jump equation is:

$$\rho^{(1)}\mathbf{u}^{(1)}\left[\left(\mathbf{u}^{(1)} - \hat{\mathbf{w}}\right)\cdot\hat{\mathbf{n}}^{(1)}\right] - \sum_{m=1}^{2}\boldsymbol{\sigma}^{(m)}\cdot\hat{\mathbf{n}}^{(m)} = \mathbf{0}. \tag{3.32}$$

3.4. Energy

In this section, three forms of single-phase energy conservation equations are developed, together with the related jump conditions.

3.4.1. Total Energy

To obtain the local and instantaneous single-phase equations and jump condition for the total energy, the conservation principle (3.1) is applied using the following quantities:

- $\phi^{(m)} = \rho^{(m)}e_t^{(m)}$ the total energy per unit volume of the phase $\mathcal{P}^{(m)}$, for $m \in \{1, 2\}$;
- $\hat{\phi} = \hat{\rho}\hat{e}$ the internal energy per unit surface of the interface Σ. The mechanical part of the surface energy can be neglected in this balance because because of the really small surface density of the interface [28];
- $\mathbf{J}^{(m)} = \mathbf{q}^{(m)} - \boldsymbol{\sigma}^{(m)}\cdot\mathbf{u}^{(m)}$, which is the sum of the total heat flux $\mathbf{q}^{(m)}$ and the flux from the work of stresses, for $m \in \{1, 2\}$. According to the assumptions (2.12) and (2.14), the total heat flux in the phase $\mathcal{P}^{(m)}$ can be written under the form [45]:

$$\mathbf{q}^{(m)} = -\lambda^{(m)}\boldsymbol{\nabla}T^{(m)} + \rho^{(m)}\sum_{k\in\Omega^{(1)}}h_k Y_k^{(m)}\mathbf{V}_k^{(m)}, \tag{3.33}$$

with $\lambda^{(m)}$ the heat conductivity of the phase $\mathcal{P}^{(m)}$, and h_k the enthalpy per unit mass of species k. Note that it is because of the property (2.12) that Eq. (3.33) consistently reduces to $\mathbf{q}^{(2)} = -\lambda^{(2)}\boldsymbol{\nabla}T^{(2)}$ in the solid phase. In the gas phase, Eq. (3.33) provides the expected expression for the total heat flux in a gas mixture [45];

- $\hat{\mathbf{J}} = \mathbf{0}$ (no surface heat diffusion and no work of the surface tension forces);
- $\Theta^{(m)} = \rho \mathbf{g} \cdot \mathbf{u}^{(m)} + \dot{\mathcal{Q}}^{(m)}$, for $m \in \{1, 2\}$. The first term is the power produced by the volume gravity force on the phase $\mathcal{P}^{(m)}$. The second term is a heat source per unit volume due, for example, to a radiative transfers in the phase $\mathcal{P}^{(m)}$;
- $\hat{\Theta} = \hat{\rho} \hat{\mathbf{w}} \cdot \mathbf{g} + \dot{\hat{\mathcal{Q}}}$. The first term is the power produced by surface gravity force on the interface Σ. The second term is a heat source per unit surface $\dot{\hat{\mathcal{Q}}}$ (as, for example, a radiative contribution) at the interface Σ.

From Eq. (3.7), we deduce the local and instantaneous equation in each phase $m \in \{1, 2\}$ [45]:

$$\frac{\partial \left(\rho^{(m)} e_t^{(m)} \right)}{\partial t} + \boldsymbol{\nabla} \cdot \left(\rho^{(m)} \mathbf{u}^{(m)} e_t^{(m)} \right) = -\boldsymbol{\nabla} \cdot \mathbf{q}^{(m)} + \boldsymbol{\nabla} \cdot \left(\boldsymbol{\sigma}^{(m)} \cdot \mathbf{u}^{(m)} \right) + \dot{\mathcal{Q}}^{(m)} + \rho^{(m)} \mathbf{g} \cdot \mathbf{u}^{(m)} \text{ in the phase } \mathcal{P}^{(m)}. \tag{3.34}$$

According to Eq. (3.9), the solution of these local equations shall satisfy the following jump condition:

$$\rho^{(1)} e_t^{(1)} \left[\mathbf{u}^{(1)} - \hat{\mathbf{w}} \right] \cdot \hat{\mathbf{n}}^{(1)} + \sum_{m=1}^{2} \left[\mathbf{q}^{(m)} - \boldsymbol{\sigma}^{(m)} \cdot \mathbf{u}^{(m)} \right] \cdot \hat{\mathbf{n}}^{(m)} = \frac{\mathrm{d} \left(\hat{\rho} \hat{e} \right)}{\mathrm{d}t} - \hat{\rho} \hat{\mathbf{w}} \cdot \mathbf{g} - \dot{\hat{\mathcal{Q}}} \text{ at the interface.} \tag{3.35}$$

The contribution of the interface weight is considered to be negligible, so the retained jump equation is:

$$\rho^{(1)} e_t^{(1)} \left[\mathbf{u}^{(1)} - \hat{\mathbf{w}} \right] \cdot \hat{\mathbf{n}}^{(1)} + \sum_{m=1}^{2} \left[\mathbf{q}^{(m)} - \boldsymbol{\sigma}^{(m)} \cdot \mathbf{u}^{(m)} \right] \cdot \hat{\mathbf{n}}^{(m)} = \frac{\mathrm{d} \left(\hat{\rho} \hat{e} \right)}{\mathrm{d}t} - \dot{\hat{\mathcal{Q}}} \text{ at the interface } \Sigma. \tag{3.36}$$

At this point, the total derivative of the surface energy has to be made explicit. According to the approximation of perfect mixture for the surface phase, the internal energy per unit surface, $\hat{\rho} \hat{e}$, may be written as the sum of two contributions as follows:

$$\hat{\rho} \hat{e} = \sum_{k \in \Omega^{(\Sigma)}} \hat{\rho}_k e_k + \widehat{[X_*]} e_{\mathrm{mol},*} \tag{3.37}$$

where e_k is the internal energy per unit mass of the species k, $\hat{\rho}_k$ is the surface density of the species k, $\widehat{[X_*]}$ is the surface molar concentration of vacant site, and $e_{\mathrm{mol},*}$ is the internal energy per mole of vacant sites. The total derivative of (3.37) is then computed:

$$\frac{\mathrm{d} \left(\hat{\rho} \hat{e} \right)}{\mathrm{d}t} = \sum_{k \in \Omega^{(\Sigma)}} W_k \dot{\hat{s}}_k e_k + \dot{\hat{s}}_* e_{\mathrm{mol},*} + \frac{\mathrm{d}T}{\mathrm{d}t} \left(\sum_{k \in \Omega^{(\Sigma)}} \hat{\rho}_k \frac{\mathrm{d}e_k}{\mathrm{d}T} + \widehat{[X_*]} \frac{\mathrm{d}e_{\mathrm{mol},*}}{\mathrm{d}T} \right). \tag{3.38}$$

Because of the small concentrations per unit area at the surface, the heat capacity term can be safely neglected in Eq. (3.38), and the equation reduces to

$$\frac{\mathrm{d} \left(\hat{\rho} \hat{e} \right)}{\mathrm{d}t} = \sum_{k \in \Omega^{(\Sigma)}} W_k \dot{\hat{s}}_k e_k + \dot{\hat{s}}_* e_{\mathrm{mol},*}. \tag{3.39}$$

Finally by injecting Eq. (3.39) into Eq. (3.36) the following jump equation for the total energy is obtained:

$$\rho^{(1)} e_t^{(1)} \left[\mathbf{u}^{(1)} - \hat{\mathbf{w}} \right] \cdot \hat{\mathbf{n}}^{(1)} + \sum_{m=1}^{2} \left[\mathbf{q}^{(m)} - \boldsymbol{\sigma}^{(m)} \cdot \mathbf{u}^{(m)} \right] \cdot \hat{\mathbf{n}}^{(m)} = \sum_{k \in \Omega^{(\Sigma)}} W_k e_k \dot{\hat{s}}_k + e_{\mathrm{mol},*} \dot{\hat{s}}_* - \dot{\hat{\mathcal{Q}}} \text{ at the interface } \Sigma. \tag{3.40}$$

3.4.2. Enthalpy

In each phase $\mathcal{P}^{(m)}$, the enthalpy is defined as

$$h^{(m)} = e_t^{(m)} - \frac{1}{2}\mathbf{u}^{(m)} \cdot \mathbf{u}^{(m)} + \frac{P^{(m)}}{\rho^{(m)}}. \tag{3.41}$$

From the local equations of the total energy (3.34), we can demonstrate that the enthalpies $\left(h^{(m)}\right)_{m\in\{1,2\}}$ respectively verifie the local equations [45]:

$$\frac{\partial\left(\rho^{(m)}h^{(m)}\right)}{\partial t} + \boldsymbol{\nabla}\cdot\left(\rho^{(m)}h^{(m)}\mathbf{u}^{(m)}\right) = \frac{\mathrm{d}P^{(m)}}{\mathrm{d}t} - \boldsymbol{\nabla}\cdot\mathbf{q}^{(m)} + \boldsymbol{\tau}^{(m)} : \boldsymbol{e}^{(m)} + \dot{\mathcal{Q}}^{(m)} \quad \text{in the phase } \mathcal{P}^{(m)}. \tag{3.42}$$

where for $m \in \{1,2\}$

- $\boldsymbol{\tau}^{(m)}$ is the viscous part of the stress tensor $\boldsymbol{\sigma}^{(m)}$ in the phase $\mathcal{P}^{(m)}$ (3.27):

$$\boldsymbol{\tau} = \boldsymbol{\sigma}^{(m)} + P^{(m)}\mathbf{I} = \mu^{(m)}\left(\boldsymbol{\nabla}\mathbf{u}^{(m)} + \boldsymbol{\nabla}^\top\mathbf{u}^{(m)} - \frac{2}{3}\left(\boldsymbol{\nabla}\cdot\mathbf{u}^{(m)}\right)\mathbf{I}\right) + \kappa^{(m)}\left(\boldsymbol{\nabla}\cdot\mathbf{u}^{(m)}\right)\mathbf{I}. \tag{3.43}$$

- $\boldsymbol{e}^{(m)}$ is the rate-of-strain tensor in the phase $\mathcal{P}^{(m)}$:

$$\boldsymbol{e}^{(m)} = \frac{1}{2}\left(\boldsymbol{\nabla}\mathbf{u}^{(m)} + \boldsymbol{\nabla}^\top\mathbf{u}^{(m)}\right). \tag{3.44}$$

The local instantaneous jump equation for total energy (3.40) can be re-written to make the enthalpies $\left(h^{(m)}\right)_{m\in\{1,2\}}$ appear:

$$\left[\rho^{(1)}\left(h^{(1)} + \frac{1}{2}\mathbf{u}^{(1)}\cdot\mathbf{u}^{(1)} - \frac{P^{(1)}}{\rho^{(1)}}\right)\left(\mathbf{u}^{(1)} - \hat{\mathbf{w}}\right)\right]\cdot\hat{\mathbf{n}}^{(1)} + \sum_{m=1}^{2}\left[\mathbf{q}^{(m)} - \boldsymbol{\sigma}^{(m)}\cdot\mathbf{u}^{(m)}\right]\cdot\hat{\mathbf{n}}^{(m)} = \sum_{k\in\Omega^{(\Sigma)}} W_k e_k \dot{\hat{s}}_k + e_{\mathrm{mol},*}\dot{\hat{s}}_* - \dot{\hat{\mathcal{Q}}} \quad \text{at } \Sigma. \tag{3.45}$$

In Eq. (3.45), the term $-P^{(1)}\mathbf{u}^{(1)}\cdot\hat{\mathbf{n}}^{(1)}$ cancels out with the pressure contribution of the stress tensor, and using the relation Eq. (3.19), we have:

$$\begin{cases} \left[\rho^{(1)}\left(h^{(1)} + \frac{1}{2}\mathbf{u}^{(1)}\cdot\mathbf{u}^{(1)}\right)\left(\mathbf{u}^{(1)} - \hat{\mathbf{w}}\right)\right]\cdot\hat{\mathbf{n}}^{(1)} + \displaystyle\sum_{m=1}^{2}\left[\mathbf{q}^{(m)} - \boldsymbol{\tau}^{(m)}\cdot\mathbf{u}^{(m)} + P^{(m)}\hat{\mathbf{w}}\right]\cdot\hat{\mathbf{n}}^{(m)} \\ \qquad\qquad = \displaystyle\sum_{k\in\Omega^{(\Sigma)}} W_k e_k \dot{\hat{s}}_k + e_{\mathrm{mol},*}\dot{\hat{s}}_* - \dot{\hat{\mathcal{Q}}} \quad \text{at } \Sigma \end{cases}. \tag{3.46}$$

By using Eq. (3.14) the following equation can be derived:

$$\rho^{(1)}h^{(1)}\left(\mathbf{u}^{(1)} - \hat{\mathbf{w}}\right)\cdot\hat{\mathbf{n}}^{(1)} + \rho^{(1)}\sum_{k\in\Omega^{(1)}} h_k Y_k^{(1)}\mathbf{V}_k^{(1)}\cdot\hat{\mathbf{n}}^{(1)} = -\sum_{k\in\Omega^{(1)}} h_k W_k \dot{\hat{s}}_k \quad \text{at } \Sigma \tag{3.47}$$

so that thanks to the definition of the total heat flux (3.33), we can rewrite (3.46) as:

$$\begin{aligned} &\left[\rho^{(1)}\left(\frac{1}{2}\mathbf{u}^{(1)}\cdot\mathbf{u}^{(1)}\right)\left(\mathbf{u}^{(1)} - \hat{\mathbf{w}}\right)\right]\cdot\hat{\mathbf{n}}^{(1)} + \sum_{m=1}^{2}\left[P^{(m)}\hat{\mathbf{w}} - \boldsymbol{\tau}^{(m)}\cdot\mathbf{u}^{(m)} - \lambda^{(m)}\boldsymbol{\nabla}T^{(m)}\right]\cdot\hat{\mathbf{n}}^{(m)} \\ &= \\ &\sum_{k\in\Omega^{(\Sigma)}} e_k W_k \dot{\hat{s}}_k + e_{\mathrm{mol},*}\dot{\hat{s}}_* + \sum_{k\in\Omega^{(1)}} h_k W_k \dot{\hat{s}}_k - \dot{\hat{\mathcal{Q}}} \quad \text{at } \Sigma. \end{aligned} \tag{3.48}$$

Eq. (3.48) is consistent with the boundary condition for a motionless interface ($\mathbf{u}^{(2)}\big|_{\Sigma} = \hat{\mathbf{w}} = \mathbf{0}$) derived in [9] from a balance of non-chemical energy at the gas-solid interface, as long as the internal energy of surface species is identified with their enthalpy:

$$\forall k \in \Omega^{(\Sigma)},\ e_k = h_k \quad \& \quad e_{\mathrm{mol},*} = h_{\mathrm{mol},*} \tag{3.49}$$

Eq. (3.49) is explicitly assumed in Cantera, see the Doxygen documentation [1]. Indeed, if the following additional approximations are made:

$$\begin{cases} \left[\boldsymbol{\tau}^{(1)} \cdot \mathbf{u}^{(1)}\right] \cdot \hat{\mathbf{n}}^{(1)} \simeq 0 \\ \dfrac{1}{2}\left(\mathbf{u}^{(1)} \cdot \mathbf{u}^{(1)}\right)\left[\mathbf{u}^{(1)} - \hat{\mathbf{w}}\right] \cdot \hat{\mathbf{n}}^{(1)} \simeq 0 \end{cases} \tag{3.50}$$

then Eq. (3.48) is consistent with the flux-matching condition at a motionless gas-solid interface introduced in [14, 13, 34][3]and used in Cantera.

3.4.3. Temperature

In the gas phase $\mathcal{P}^{(1)}$, the local equation for enthalpy (3.41) can be recast as an equation for temperature [45]:

$$\rho^{(1)} C_p^{(1)} \frac{\mathrm{d}T^{(1)}}{\mathrm{d}t} = \begin{cases} \left(\dot{\omega}'_T\right)^{(1)} + \dfrac{\mathrm{d}P^{(1)}}{\mathrm{d}t} - \left(\rho^{(1)} \displaystyle\sum_{k \in \Omega^{(1)}} C_{pk} Y_k^{(1)} \mathbf{V}_k^{(1)}\right) \cdot \boldsymbol{\nabla} T^{(1)} \\ + \boldsymbol{\nabla} \cdot \left(\lambda^{(1)} \boldsymbol{\nabla} T^{(1)}\right) + \boldsymbol{\tau}^{(1)} : \boldsymbol{e}^{(1)} + \dot{\mathcal{Q}}^{(1)} \end{cases} \tag{3.51}$$

In the solid phase $\mathcal{P}^{(2)}$, modeled as a highly viscous fluid with zero thermal expansion coefficient, the local equation for enthalpy (3.41) becomes [8]:

$$\rho^{(2)} C_p^{(2)} \frac{\mathrm{d}T^{(2)}}{\mathrm{d}t} = \boldsymbol{\nabla} \cdot \left(\lambda^{(2)} \boldsymbol{\nabla} T^{(2)}\right) + \boldsymbol{\tau}^{(2)} : \boldsymbol{e}^{(2)}. \tag{3.52}$$

In the previous equations, for $m \in \{1, 2\}$, $C_p^{(m)}$ is the mass heat capacity at constant pressure in the phase $\mathcal{P}^{(m)}$, C_{pk} is the mass heat capacity at constant pressure of species k, $\boldsymbol{e}^{(m)}$ is the rate-of-strain tensor in the phase $\mathcal{P}^{(m)}$, and $\left(\dot{\omega}'_T\right)^{(m)}$ is the heat release in the phase $\mathcal{P}^{(m)}$ due to homogeneous reactions:

$$\begin{cases} \left(\dot{\omega}'_T\right)^{(1)} = -\displaystyle\sum_{k \in \Omega^{(1)}} h_k \dot{\omega}_k^{(1)} \\ \left(\dot{\omega}'_T\right)^{(2)} = 0 \end{cases} \tag{3.53}$$

Moreover, we introduce the thermal expansion coefficient $\beta^{(m)}$ in the phase m as

$$\begin{cases} \beta^{(1)} = \dfrac{1}{T^{(1)}} & \text{in the gas phase} \\ \beta^{(2)} = 0 & \text{in the solid phase.} \end{cases} \tag{3.54}$$

Single-phase equations (3.51) and (3.52) can then be written in an unified way:

$$\rho^{(m)} C_p^{(m)} \frac{\mathrm{d}T^{(m)}}{\mathrm{d}t} = \begin{cases} \left(\dot{\omega}'_T\right)^{(m)} + \beta^{(m)} T^{(m)} \dfrac{\mathrm{d}P^{(m)}}{\mathrm{d}t} - \left(\rho^{(m)} \displaystyle\sum_{k \in \Omega^{(1)}} C_{pk} Y_k^{(m)} \mathbf{V}_k^{(m)}\right) \cdot \boldsymbol{\nabla} T^{(m)} \\ + \boldsymbol{\nabla} \cdot \left(\lambda^{(m)} \boldsymbol{\nabla} T^{(m)}\right) + \boldsymbol{\tau}^{(m)} : \boldsymbol{e}^{(m)} + \dot{\mathcal{Q}}^{(m)} \end{cases} \tag{3.55}$$

because of Eqs. (2.12), (3.54), (3.54), and the additional relation that applies in the solid phase $\mathcal{P}^{(2)}$:

$$\dot{\mathcal{Q}}^{(2)} = 0 \tag{3.56}$$

[3]In these references, the vacant surface sites are treated as a surface species, so that the term $e_{\mathrm{mol},*}\dot{\hat{s}}_*$ is included in the sum over the surface species.

3.5. Constitutive relations

This work deals with the theoretical formalism used to describe gas-particle reactive flows in the presence of surface reaction, in the frame of a one-fluid approach. Its derivation is independent of the constitutive relations used to close the unclosed terms appearing in the system of equations. This section aims to provide references about those constitutive relations commonly used in the frame of the DNS combustion.

The solid phase requires to specify its thermal conductivity $\lambda^{(2)}$, heat capacity $C_p^{(2)}$ density $\rho^{(2)}$, which are known for a variety of materials and temperature range.

For the reacting gas phase, modelling aspects and their availability/suitability are extensively discussed in [45, 23, 34]. The models concern:

- the chemical kinetic scheme: what are the involved gas species, the chemical reactions that occur between them, and the rate of these reactions. Its knowledge enables to compute the gas-species mass rates $\dot{\omega}_k^{(1)}$;
- thermodynamic quantities: how to compute gas-species heat capacities C_{pk} and enthalpies h_k;
- transport phenomena: how to compute the local viscosity $\mu^{(1)}$, the thermal conductivity $\lambda^{(1)}$ and the diffusion velocities of gas species $\mathbf{V}_k^{(1)}$ with respect to the local thermodynamical state of the gas mixture.

The numerical evaluation of these models requires the knowledge of some tabulated data, that are available for a large number of fuels and operating conditions.

Closures related to the gas-solid interface phenomena are the most uncertain part of the modelling, as surface chemistry is currently less known than gas-phase chemistry. Along a value for the density of surface sites $\hat{\Gamma}$, a chemical kinetic scheme and thermodynamic properties should be specified at the reacting surface. General relations for surface kinetics and thermodynamics are described in [13, 34]. Their numerical evaluation requires the knowledge of some tabulated data. A selection of such available data is provided in the fourth chapter of [20].

For both gas-phase and surface modelling, the open-source software Cantera [25] provides a convenient solution to exchange the necessary tabulated data under a standard format (based on YAML), and to numerically evaluate the corresponding models.

4. Single-field representation

In this section, the two-field description previously derived in Section 3 is recast as a *single-field representation*, following the approach of Kataoka [33].

4.1. General approach

Let us derive the single-field representation in a generic way for a conservative quantity. The single-phase local conservation equations (3.7) can be multiplied by the phase function $\chi^{(m)}$ and summed over m to obtain:

$$\sum_{m=1}^{2} \chi^{(m)} \left(\frac{\partial \phi^{(m)}}{\partial t} + \boldsymbol{\nabla} \cdot \left(\phi^{(m)} \mathbf{u}^{(m)} \right) \right) = - \sum_{m=1}^{2} \chi^{(m)} \boldsymbol{\nabla} \cdot \mathbf{J}^{(m)} + \sum_{m=1}^{2} \chi^{(m)} \Theta^{(m)}. \tag{4.1}$$

Using the expression of the partial derivatives of the characteristic phase functions (i.e. Eqs. (2.5)), the following generic relations can be demonstrated

$$\begin{cases} \chi^{(m)} \dfrac{\partial \phi^{(m)}}{\partial t} = \dfrac{\partial \left(\chi^{(m)} \phi^{(m)} \right)}{\partial t} - \delta_\Sigma \phi^{(m)} \hat{\mathbf{w}} \cdot \hat{\mathbf{n}}^{(m)} \\ \chi^{(m)} \boldsymbol{\nabla} \cdot \left(\mathbf{u}^{(m)} \phi^{(m)} \right) = \boldsymbol{\nabla} \cdot \left(\chi^{(m)} \phi^{(m)} \mathbf{u}^{(m)} \right) + \delta_\Sigma \phi^{(m)} \mathbf{u}^{(m)} \cdot \hat{\mathbf{n}}^{(m)}, \end{cases} \tag{4.2}$$

which lead to write

$$\chi^{(m)}\left(\frac{\partial\phi^{(m)}}{\partial t}+\boldsymbol{\nabla}\cdot\left(\mathbf{u}^{(m)}\phi^{(m)}\right)\right)=\frac{\partial\left(\chi^{(m)}\phi^{(m)}\right)}{\partial t}+\boldsymbol{\nabla}\cdot\left(\chi^{(m)}\phi^{(m)}\mathbf{u}^{(m)}\right)+\delta_\Sigma\phi^{(m)}\left(\mathbf{u}^{(m)}-\hat{\mathbf{w}}\right)\cdot\hat{\mathbf{n}}^{(m)}. \quad (4.3)$$

Similar algebra provides:

$$\chi^{(m)}\boldsymbol{\nabla}\cdot\mathbf{J}^{(m)}=\boldsymbol{\nabla}\cdot\left(\chi^{(m)}\mathbf{J}^{(m)}\right)+\delta_\Sigma\mathbf{J}^{(m)}\cdot\hat{\mathbf{n}}^{(m)}. \quad (4.4)$$

Moreover, a direct consequence of Eq. (2.8) is that

$$\sum_{m=1}^{2}\chi^{(m)}\phi^{(m)}\mathbf{u}^{(m)}=\phi\mathbf{u}. \quad (4.5)$$

Applying Eqs. (4.3), (4.4) and (2.8) to Eq. (4.1), we obtain

$$\frac{\partial\phi}{\partial t}+\boldsymbol{\nabla}\cdot(\phi\mathbf{u})=-\boldsymbol{\nabla}\cdot\mathbf{J}+\Theta-\delta_\Sigma\left(\sum_{m=1}^{2}\left[\phi^{(m)}\left(\mathbf{u}^{(m)}-\hat{\mathbf{w}}\right)+\mathbf{J}^{(m)}\right]\cdot\hat{\mathbf{n}}^{(m)}\right). \quad (4.6)$$

Finally, by inserting the general jump equation (3.8) in Eq. (4.6) with the assumption of a rigid interface, the general form of the single-fluid representation for a conservative quantity is obtained:

$$\frac{\partial\phi}{\partial t}+\boldsymbol{\nabla}\cdot(\phi\mathbf{u})=-\boldsymbol{\nabla}\cdot\mathbf{J}+\Theta-\delta_\Sigma\left(\frac{\mathrm{d}\hat{\phi}}{\mathrm{d}t}+\boldsymbol{\nabla}_\Sigma\cdot\hat{\mathbf{J}}-\hat{\Theta}\right). \quad (4.7)$$

As demonstrated by Kataoka [33], we have the strict equivalence:

$$\text{Eq. (4.7)} \iff \begin{cases}\text{Eq. (3.7) for } m\in\{1,2\}\\ \text{Eq. (3.8).}\end{cases} \quad (4.8)$$

4.2. Species and mass

Let $k\in[\![1,K]\!]$. We apply Eq. (4.7) in the context of the species balance established in Sec. 3.2 to obtain

$$\forall k\in[\![1,K]\!],\quad \frac{\partial}{\partial t}(\rho Y_k)+\boldsymbol{\nabla}\cdot\left(\rho Y_k\left(\mathbf{u}+\mathbf{V}_k\right)\right)=\dot{\omega}_k-\delta_\Sigma\left(\frac{\mathrm{d}\hat{\rho}_k}{\mathrm{d}t}-W_k\dot{\hat{s}}_k.\right) \quad (4.9)$$

Let us specify the form of Eq. (4.9) in the special cases of k corresponding to either a gas species, a solid species or a surface species.

4.2.1. Gas species

Let us take the special case of a gas species, *i.e.* $k\in\Omega^{(1)}$. According to Eq. (2.12), Eq. (4.9) simplifies into:

$$\forall k\in\Omega^{(1)},\quad \frac{\partial}{\partial t}(\rho Y_k)+\boldsymbol{\nabla}\cdot\left(\rho Y_k\left(\mathbf{u}+\mathbf{V}_k\right)\right)=\dot{\omega}_k+\delta_\Sigma W_k\dot{\hat{s}}_k. \quad (4.10)$$

If Eq. (4.10) is summed over the gas species $k\in\Omega^{(1)}$ and by using Eq. (2.12) and Eq. (2.11), we obtain the single-field representation for the gas mass:

$$\frac{\partial}{\partial t}\left(\chi^{(1)}\rho\right)+\boldsymbol{\nabla}\cdot\left(\chi^{(1)}\rho\mathbf{u}\right)=\delta_\Sigma\sum_{k\in\Omega^{(1)}}W_k\dot{\hat{s}}_k. \quad (4.11)$$

4.2.2. Solid species

Let us take the special case of a solid species, *i.e.* $k = k_s$. According to Eq. (2.14) and Eq. (2.13), Eq. (4.9) simplifies into:

$$\frac{\partial}{\partial t}\Big(\chi^{(2)}\rho\Big) + \boldsymbol{\nabla}\cdot\Big(\chi^{(2)}\rho\mathbf{u}\Big) = 0. \tag{4.12}$$

Since the solid density $\rho^{(2)}$ is actually a constant, Eq. (4.12) simplifies into

$$\frac{\partial}{\partial t}\Big(\chi^{(2)}\Big) + \boldsymbol{\nabla}\cdot\Big(\chi^{(2)}\mathbf{u}\Big) = 0. \tag{4.13}$$

4.2.3. Mass

If Eq. (4.11) and Eq. (4.12) are added together, the single-field representation for the two-phase density is obtained:

$$\frac{\partial\rho}{\partial t} + \boldsymbol{\nabla}\cdot(\rho\mathbf{u}) = \delta_\Sigma\left(\sum_{k\in\Omega^{(1)}} W_k\dot{\hat{s}}_k\right) \tag{4.14}$$

Thanks to Eq. (3.22), the singular term in (4.14) can be equivalently written as

$$\delta_\Sigma\left(\sum_{k\in\Omega^{(1)}} W_k\dot{\hat{s}}_k\right) = -\delta_\Sigma\left(\frac{\mathrm{d}\hat{\rho}}{\mathrm{d}t}\right) = -\delta_\Sigma\left(\sum_{k\in\Omega^{(\Sigma)}} W_k\dot{\hat{s}}_k\right). \tag{4.15}$$

4.3. Momentum

The general approach developed in Sec. 4.1 can be applied to the conservation of a vector quantity. The single-field representation associated with the generic single-phase equations (3.25) and the generic jump equation (3.26) then writes:

$$\frac{\partial\boldsymbol{\phi}}{\partial t} + \boldsymbol{\nabla}\cdot(\boldsymbol{\phi}\mathbf{u}) = \boldsymbol{\nabla}\cdot\boldsymbol{J} + \boldsymbol{\Theta} - \delta_\Sigma\left(\frac{\mathrm{d}\hat{\boldsymbol{\phi}}}{\mathrm{d}t} + \boldsymbol{\nabla}_\Sigma\hat{J} - (\boldsymbol{\nabla}_\Sigma\cdot\hat{\mathbf{n}})\,\hat{J}\hat{\mathbf{n}} - \hat{\boldsymbol{\Theta}}\right). \tag{4.16}$$

Applying Eq. (4.16) in the context of the balance of momentum established in Section 3.3, the local single-phase equations (3.30) for $m \in \{1, 2\}$ and the jump equation (3.32) are equivalent to the single field representation:

$$\frac{\partial}{\partial t}(\rho\mathbf{u}) + \boldsymbol{\nabla}\cdot(\rho\mathbf{u}\mathbf{u}) = \boldsymbol{\nabla}\cdot\boldsymbol{\sigma} + \rho\mathbf{g} \tag{4.17}$$

4.4. Energy

In the following, the single-field representations for total energy, enthalpy, and temperature are successively derived.

4.4.1. Total energy

Using Eq. (4.7) in the context of the energy balance established in Sec. 3.4, the local single-phase equations (3.34) for $m \in \{1, 2\}$ and the jump equation (3.40) are shown to be equivalent to the single-field representation:

$$\frac{\partial}{\partial t}(\rho e_t) + \boldsymbol{\nabla}\cdot(\rho e_t\mathbf{u}) = -\boldsymbol{\nabla}\cdot\mathbf{q} + \dot{\mathcal{Q}} + \boldsymbol{\nabla}\cdot\big[\boldsymbol{\sigma}\cdot\mathbf{u}\big] + \rho\mathbf{g}\cdot\mathbf{u} + \delta_\Sigma\left(-\sum_{k\in\Omega^{(\Sigma)}} W_k e_k\dot{\hat{s}}_k - e_{\mathrm{mol},*}\dot{\hat{s}}_* + \dot{\hat{\mathcal{Q}}}\right). \tag{4.18}$$

4.4.2. Enthalpy

Starting from the single-phase local equations for enthalpy (3.42), we can write

$$\sum_{m=1}^{2}\chi^{(m)}\left[\frac{\partial\left(\rho^{(m)}h^{(m)}\right)}{\partial t}+\boldsymbol{\nabla}\cdot\left(\rho^{(m)}h^{(m)}\mathbf{u}^{(m)}\right)\right]=\sum_{m=1}^{2}\chi^{(m)}\left[\frac{\mathrm{d}P^{(m)}}{\mathrm{d}t}-\boldsymbol{\nabla}\cdot\mathbf{q}^{(m)}+\boldsymbol{\tau}^{(m)}:\boldsymbol{e}^{(m)}+\dot{\mathcal{Q}}^{(m)}\right]. \tag{4.19}$$

The left-hand side (LHS) can be rewritten using Eq. (4.3). In the right-hand side (RHS), the pressure term can be treated with Eq. (B.2), the flux term with Eq. (4.4), the viscous dissipation term with Eqs (2.8) and (2.6), and the radiative source term with Eq. (2.6). We then obtain:

$$\frac{\partial\left(\rho h\right)}{\partial t}+\boldsymbol{\nabla}\cdot\left(\rho h\mathbf{u}\right)=\begin{cases}\dfrac{\partial P}{\partial t}-\delta_{\Sigma}\hat{\mathbf{w}}\cdot\displaystyle\sum_{m=1}^{2}P^{(m)}\hat{\mathbf{n}}^{(m)}+\mathbf{u}\cdot\left(\boldsymbol{\nabla}P+\delta_{\Sigma}\displaystyle\sum_{m=1}^{2}P^{(m)}\hat{\mathbf{n}}^{(m)}\right)\\ -\boldsymbol{\nabla}\cdot\mathbf{q}+\boldsymbol{\tau}:\boldsymbol{e}+\dot{\mathcal{Q}}\\ -\delta_{\Sigma}\left(\rho^{(1)}h^{(1)}\left(\mathbf{u}^{(1)}-\hat{\mathbf{w}}\right)\cdot\mathbf{n}^{(1)}+\displaystyle\sum_{m=1}^{2}\mathbf{q}^{(m)}\cdot\mathbf{n}^{(m)}\right).\end{cases} \tag{4.20}$$

Inserting the jump equation (3.46) into Eq. (4.20), we obtain the single field representation for enthalpy:

$$\frac{\partial\left(\rho h\right)}{\partial t}+\boldsymbol{\nabla}\cdot\left(\rho h\mathbf{u}\right)=\begin{cases}\dfrac{\partial P}{\partial t}+\mathbf{u}\cdot\left(\boldsymbol{\nabla}P+\delta_{\Sigma}\displaystyle\sum_{m=1}^{2}P^{(m)}\mathbf{n}^{(m)}\right)\\ -\boldsymbol{\nabla}\cdot\mathbf{q}+\boldsymbol{\tau}:\boldsymbol{e}+\dot{\mathcal{Q}}\\ \delta_{\Sigma}\left(\begin{array}{l}\left[\rho^{(1)}\left(\dfrac{1}{2}\mathbf{u}^{(1)}\cdot\mathbf{u}^{(1)}\right)\left(\mathbf{u}^{(1)}-\hat{\mathbf{w}}\right)\right]\cdot\mathbf{n}^{(1)}\\ -\displaystyle\sum_{m=1}^{2}\left[\boldsymbol{\tau}^{(m)}\cdot\mathbf{u}^{(m)}\right]\cdot\mathbf{n}^{(m)}-\sum_{k\in\Omega^{(\Sigma)}}W_k e_k\dot{\hat{s}}_k-e_{\mathrm{mol},*}\dot{\hat{s}}_*+\dot{\hat{\mathcal{Q}}}\end{array}\right).\end{cases} \tag{4.21}$$

4.4.3. Temperature

To obtain the single-field representation for the temperature, we apply the procedure described in 4.1 to the local single-phase equations (3.55). The first step writes:

$$\sum_{m=1}^{2}\rho^{(m)}C_p^{(m)}\chi^{(m)}\frac{\mathrm{d}T^{(m)}}{\mathrm{d}t}=\sum_{m=1}^{2}\chi^{(m)}\begin{cases}\left(\dot{\omega}_T'\right)^{(m)}+\beta^{(m)}T^{(m)}\dfrac{\mathrm{d}P^{(m)}}{\mathrm{d}t}-\left(\displaystyle\sum_{k\in\Omega^{(1)}}\rho^{(m)}C_{pk}Y_k^{(m)}\mathbf{V}_k^{(m)}\right)\cdot\boldsymbol{\nabla}T^{(m)}\\ +\boldsymbol{\nabla}\cdot\left(\lambda^{(m)}\boldsymbol{\nabla}T^{(m)}\right)+\boldsymbol{\tau}^{(m)}:\boldsymbol{e}^{(m)}+\dot{\mathcal{Q}}^{(m)}.\end{cases} \tag{4.22}$$

The LHS of Eq. (4.22) can be rewritten thanks to Eqs. (2.8) and (B.1), and the continuity of temperature at the interface Σ:

$$\sum_{m=1}^{2}\chi^{(m)}\rho^{(m)}C_p^{(m)}\frac{\mathrm{d}T^{(m)}}{\mathrm{d}t}=\rho C_p\left(\frac{\partial T}{\partial t}+\mathbf{u}\cdot\boldsymbol{\nabla}T\right). \tag{4.23}$$

In the RHS of Eq. (4.22), the terms needing a special treatment are

- the sum on gas species, that can be expressed as

$$\sum_{m=1}^{2}\chi^{(m)}\sum_{k\in\Omega^{(1)}}\rho^{(m)}C_{pk}Y_k^{(m)}\mathbf{V}_k^{(m)}\cdot\boldsymbol{\nabla}T^{(m)} = \sum_{k\in\Omega^{(1)}}\rho C_{pk}Y_k\mathbf{V}_k\cdot\left(\boldsymbol{\nabla}T+\delta_\Sigma\left[\sum_{m=1}^{2}T^{(m)}\hat{\mathbf{n}}^{(m)}\right]\right)$$
$$= \sum_{k\in\Omega^{(1)}}\rho C_{pk}Y_k\mathbf{V}_k\cdot\boldsymbol{\nabla}T. \tag{4.24}$$

- the Fourier term

$$\sum_{m=1}^{2}\chi^{(m)}\boldsymbol{\nabla}\cdot\left(\lambda^{(m)}\boldsymbol{\nabla}T^{(m)}\right) = \boldsymbol{\nabla}\cdot\left(\sum_{m=1}^{2}\chi^{(m)}\lambda^{(m)}\boldsymbol{\nabla}T^{(m)}\right)-\sum_{m=1}^{2}\lambda^{(m)}\boldsymbol{\nabla}T^{(m)}\cdot\boldsymbol{\nabla}\chi^{(m)}$$
$$= \boldsymbol{\nabla}\cdot\left(\lambda\left(\boldsymbol{\nabla}T+\delta_\Sigma\sum_{m=1}^{2}T^{(m)}\hat{\mathbf{n}}^{(m)}\right)\right)+\delta_\Sigma\sum_{m=1}^{2}\lambda^{(m)}\boldsymbol{\nabla}T^{(m)}\cdot\hat{\mathbf{n}}^{(m)}$$
$$\implies \sum_{m=1}^{2}\chi^{(m)}\boldsymbol{\nabla}\cdot\left(\lambda^{(m)}\boldsymbol{\nabla}T^{(m)}\right) = \boldsymbol{\nabla}\cdot(\lambda\boldsymbol{\nabla}T)+\delta_\Sigma\sum_{m=1}^{2}\lambda^{(m)}\boldsymbol{\nabla}T^{(m)}\cdot\hat{\mathbf{n}}^{(m)} \tag{4.25}$$

  where $\boldsymbol{\nabla}T^{(m)}$ at the interface is given by Eq. (2.7).

- the pressure term: because of Eq. (3.54), we have

$$\sum_{m=1}^{2}\chi^{(m)}\beta^{(m)}T^{(m)} = \chi^{(1)} \tag{4.26}$$

  so that

$$\sum_{m=1}^{2}\chi^{(m)}\beta^{(m)}T^{(m)}\frac{\mathrm{d}P^{(m)}}{\mathrm{d}t} = \chi^{(1)}\frac{\mathrm{d}P^{(1)}}{\mathrm{d}t}. \tag{4.27}$$

Inserting Eqs. (4.23), (4.24), (4.25) and (4.27) in Eq. (4.22) gives

$$\rho C_p\left(\frac{\partial T}{\partial t}+\mathbf{u}\cdot\boldsymbol{\nabla}T\right) = \begin{cases}\dot{\omega}'_T+\boldsymbol{\nabla}\cdot(\lambda\boldsymbol{\nabla}T)+\boldsymbol{\tau}:\boldsymbol{e}+\dot{\mathcal{Q}}\\ +\displaystyle\sum_{k\in\Omega^{(1)}}\rho C_{pk}Y_k\mathbf{V}_k\cdot\boldsymbol{\nabla}T\\ +\chi^{(1)}\dfrac{\mathrm{d}P^{(1)}}{\mathrm{d}t}\\ +\delta_\Sigma\displaystyle\sum_{m=1}^{2}\lambda^{(m)}\boldsymbol{\nabla}T^{(m)}\cdot\hat{\mathbf{n}}^{(m)}.\end{cases} \tag{4.28}$$

The interfacial term in Eq. (4.28) can be substituted using the jump relation for enthalpy (3.48):

$$\sum_{m=1}^{2}\lambda^{(m)}\boldsymbol{\nabla}T^{(m)}\cdot\hat{\mathbf{n}}^{(m)} = \begin{cases}\dot{\hat{\mathcal{Q}}}-\left(\displaystyle\sum_{k\in\Omega^{(\Sigma)}}e_kW_k\dot{\hat{s}}_k+e_{\mathrm{mol},*}\dot{\hat{s}}_*+\sum_{k\in\Omega^{(1)}}h_kW_k\dot{\hat{s}}_k\right)\\ +\left[\rho^{(1)}\left(\dfrac{1}{2}\mathbf{u}^{(1)}\cdot\mathbf{u}^{(1)}\right)\left(\mathbf{u}^{(1)}-\hat{\mathbf{w}}\right)\right]\cdot\hat{\mathbf{n}}^{(1)}\\ +\displaystyle\sum_{m=1}^{2}\left[-\boldsymbol{\tau}^{(m)}\cdot\mathbf{u}^{(m)}+P^{(m)}\hat{\mathbf{w}}\right]\cdot\hat{\mathbf{n}}^{(m)}\end{cases} \tag{4.29}$$

Finally, the RHS of Eq. (4.29) is noted $\hat{\mathcal{L}}_T$, so that the single-field representation for the temperature writes

$$\rho C_p \left(\frac{\partial T}{\partial t} + \mathbf{u} \cdot \boldsymbol{\nabla} T \right) = \begin{cases} \dot{\omega}'_T + \boldsymbol{\nabla} \cdot (\lambda \boldsymbol{\nabla} T) + \boldsymbol{\tau} : \boldsymbol{e} + \dot{\mathcal{Q}} \\ + \sum_{k \in \Omega^{(1)}} \rho C_{pk} Y_k \mathbf{V}_k \cdot \boldsymbol{\nabla} T \\ + \chi^{(1)} \dfrac{\mathrm{d}P^{(1)}}{\mathrm{d}t} \\ + \delta_\Sigma \hat{\mathcal{L}}_T \end{cases} . \tag{4.30}$$

with the surface source term $\hat{\mathcal{L}}_T$ given by

$$\hat{\mathcal{L}}_T = \begin{cases} \dot{\hat{\mathcal{Q}}} - \left(\sum_{k \in \Omega^{(\Sigma)}} e_k W_k \dot{\hat{s}}_k + e_{\mathrm{mol},*} \dot{\hat{s}}_* + \sum_{k \in \Omega^{(1)}} h_k W_k \dot{\hat{s}}_k \right) \\ + \left[\rho^{(1)} \left(\dfrac{1}{2} \mathbf{u}^{(1)} \cdot \mathbf{u}^{(1)} \right) \left(\mathbf{u}^{(1)} - \hat{\mathbf{w}} \right) \right] \cdot \hat{\mathbf{n}}^{(1)} \\ + \sum_{m=1}^{2} \left[- \boldsymbol{\tau}^{(m)} \cdot \mathbf{u}^{(m)} + P^{(m)} \hat{\mathbf{w}} \right] \cdot \hat{\mathbf{n}}^{(m)} \end{cases} \tag{4.31}$$

5. Conclusion

In this work, a single-field representation has been derived, describing a reactive gas-particle flow in the presence of both homogeneous and surface reactions. It is a set of compact equations in the meaning of distributions; each one is associated to the conservation of a physical quantity, and is rigorously equivalent to the standard two-field description consisting in two single-phase equations and a jump equation. After introducing the theoretical framework, assumptions and notations, the two-field description of the problem is first derived using the integral balance method. Then, this description of the problem is embedded into a single-field representation, thus generalizing the work of Kataoka [33] to reactive gas-particle flows involving homogeneous and surface reactions. Singular surface terms appear due to the presence of surface reactions and discontinuities at the interface. In particular, the description of surface reactions is consistent with the simplified model implemented in the Surface Chemkin [13] and Cantera software [25].

This single-field representation can be used as a starting point to derive a one-fluid formulation through spatial averaging. Future work will be devoted to the derivation of such a model, and its numerical resolution. Another prospect of this study would be to extend it by relaxing the assumption that the solid phase is non-porous, by subsequently incorporating an homogenized description of the solid porous particles through effective properties. A larger class of physical systems could therefore be described.

Declaration of competing interest

The authors have no competing interest to declare regarding the publication of this article.

Aknowledgements

This work received funding from Agence national de la recherche (ANR) through the project MIMOSAH (ANR-19-CE05-0004). It was granted access to the HPC resources of CINES/IDRIS/TGCC supercomputing centers under the allocation 2023-A0142B10864 by GENCI, and of CALMIP supercomputing center under the allocation P19017. GENCI and CALMIP are gratefully acknowledged.

Appendix A. Derivation in the sense of distributions, and surface Dirac distribution

To locate the different domains, we can define a smooth function f, that verifies:

$$\forall \mathbf{x} \in \mathbb{R}^3,\, \forall t \in \mathbb{R}^+,\, \begin{cases} f(\mathbf{x},t) > 0 & \text{if } \mathbf{x} \in \mathcal{P}^{(1)} \text{ at instant } t \\ f(\mathbf{x},t) < 0 & \text{if } \mathbf{x} \in \mathcal{P}^{(2)} \text{ at instant } t \\ f(\mathbf{x},t) = 0 & \text{if } \mathbf{x} \in \Sigma \quad \text{ at instant } t. \end{cases} \tag{A.1}$$

The characteristic phase functions (2.2) can then be related to the function f defined in Eq. (A.1):

$$\forall \mathbf{x} \in \mathbb{R}^3,\, \forall t \in \mathbb{R}^+, \quad \begin{cases} \chi^{(1)}(\mathbf{x},t) = H\left(f(\mathbf{x},t)\right) \\ \chi^{(2)}(\mathbf{x},t) = 1 - H\left(f(\mathbf{x},t)\right) \end{cases} \tag{A.2}$$

where H is the Heaviside function:

$$\forall x \in \mathbb{R}, \quad H(x) = \begin{cases} 0 \text{ if } x \leq 0 \\ 1 \text{ if } x > 0. \end{cases} \tag{A.3}$$

The outwards normal to phase m can be related to the function f defined in Eq. (A.1) by:

$$\hat{\mathbf{n}}^{(m)} = (-1)^m \frac{\boldsymbol{\nabla} f}{\|\boldsymbol{\nabla} f\|}. \tag{A.4}$$

The velocity of the interface $\hat{\mathbf{w}}$ can also be related to the function f (A.1) with the well-known relation

$$\frac{\partial f}{\partial t} + \hat{\mathbf{w}} \cdot \boldsymbol{\nabla} f = 0. \tag{A.5}$$

In the sense of distributions, the derivative of the Heaviside function H is:

$$\forall x \in \mathbb{R}^3, \quad \frac{\mathrm{d}}{\mathrm{d}x} H(x) = \delta(x) \tag{A.6}$$

where δ is the 1D Dirac distribution that is defined by its action on any continuous test function $g : \mathbb{R} \to \mathbb{R}$

$$\int_{-\infty}^{+\infty} \delta(x) g(x) \mathrm{d}x = g(0). \tag{A.7}$$

The gradient of the characteristic phase functions $\left(\chi^{(m)}\right)_{m\in\{1,2\}}$ is then obtained using Eq. (A.2) and Eq. (A.6):

$$\begin{cases} \boldsymbol{\nabla}\chi^{(1)}(\mathbf{x},t) = \quad \boldsymbol{\nabla} f(\mathbf{x},t).\delta\left(f(\mathbf{x},t)\right) \\ \boldsymbol{\nabla}\chi^{(2)}(\mathbf{x},t) = -\boldsymbol{\nabla} f(\mathbf{x},t).\delta\left(f(\mathbf{x},t)\right). \end{cases} \tag{A.8}$$

These gradients can be related to the normal vectors to the interface Σ, $\left(\hat{\mathbf{n}}^{(m)}\right)_{m\in\{1,2\}}$ and the surface Dirac distribution δ_Σ with the following theorem:

Theorem 1 (Gradient in the sense of distributions [3])**.** *Let $\phi \in \mathcal{C}^1\left(\mathbb{R}^3 \backslash \Sigma\right)$, Σ being an eventual surface of discontinuity of ϕ. The following relation is true in the sense of distributions*

$$\begin{aligned} \boldsymbol{\nabla}\phi &= \sum_{m=1}^{2} \chi^{(m)} \boldsymbol{\nabla}\phi^{(m)} + \left(\phi^{(2)} - \phi^{(1)}\right) \delta_\Sigma \hat{\mathbf{n}}^{(1)} \\ &= \sum_{m=1}^{2} \chi^{(m)} \boldsymbol{\nabla}\phi^{(m)} + \left(\phi^{(1)} - \phi^{(2)}\right) \delta_\Sigma \hat{\mathbf{n}}^{(2)} \end{aligned}$$

where $\phi^{(1)}$ and $\phi^{(2)}$ are computed at the interface Σ with Eq. (2.7)*.*

The application of Theorem 1 to $\phi = \chi^{(m)}$ then provides:

$$\boldsymbol{\nabla}\chi^{(m)} = -\hat{\mathbf{n}}^{(m)}\delta_\Sigma. \tag{A.9}$$

Thus, the notion of surface Dirac distribution coincides with the interfacial area concentration $\|\boldsymbol{\nabla} f\|\delta(f)$ introduced by Kataoka [32]. Indeed,

$$\begin{aligned} \boldsymbol{\nabla}\chi^{(m)} &= (-1)^{m+1}(\boldsymbol{\nabla} f)\delta(f) && \text{(Eq. (A.8))} \\ \implies -\hat{\mathbf{n}}^{(m)}\delta_\Sigma &= (-1)^{m+1}(\boldsymbol{\nabla} f)\delta(f) && \text{(Eq. (A.9))} \\ \implies \frac{\boldsymbol{\nabla} f}{\|\boldsymbol{\nabla} f\|}\delta_\Sigma &= (\boldsymbol{\nabla} f)\delta(f) && \text{(Eq. (A.4))} \end{aligned} \tag{A.10}$$

so that

$$\delta_\Sigma = \|\boldsymbol{\nabla} f\|\delta(f). \tag{A.11}$$

The partial derivative of the $\left(\chi^{(m)}\right)_{m\in\{1,2\}}$ with respect to time can then be expressed as:

$$\begin{aligned} \frac{\partial\chi^{(m)}}{\partial t} &= (-1)^{m+1}\frac{\partial}{\partial t}\big(H(f)\big) && \text{(Eq. (A.2))} \\ &= (-1)^{m+1}\frac{\partial f}{\partial t}\delta(f) && \text{(Eq. (A.6) + chain derivative)} \\ &= (-1)^{m}\hat{\mathbf{w}}\cdot\boldsymbol{\nabla} f\delta(f) && \text{(Eq. (A.5))} \\ &= \hat{\mathbf{w}}\cdot\hat{\mathbf{n}}^{(m)}\|\boldsymbol{\nabla} f\|\delta(f) && \text{(Eq. (A.4))} \end{aligned} \tag{A.12}$$

so that by using (A.11),

$$\frac{\partial\chi^{(m)}}{\partial t} = \hat{\mathbf{w}}\cdot\hat{\mathbf{n}}^{(m)}\delta_\Sigma. \tag{A.13}$$

Appendix B. A useful relation

Using the expression for the partial derivatives of the characteristic phase functions, Eq. (2.5) and Eq. (2.8), we can demonstrate for any single-phase fields $\left(\phi^{(m)}\right)_{m\in\{1,2\}}$:

$$\chi^{(m)}\left(\frac{\partial\phi^{(m)}}{\partial t} + \mathbf{u}^{(m)}\cdot\boldsymbol{\nabla}\phi^{(m)}\right) = \frac{\partial\left(\chi^{(m)}\phi^{(m)}\right)}{\partial t} - \delta_\Sigma\phi^{(m)}\hat{\mathbf{w}}\cdot\hat{\mathbf{n}}^{(m)} + \chi^{(m)}\mathbf{u}^{(m)}\cdot\left(\boldsymbol{\nabla}\left(\chi^{(m)}\phi^{(m)}\right) + \delta_\Sigma\phi^{(m)}\hat{\mathbf{n}}^{(m)}\right) \tag{B.1}$$

As a consequence, we have:

$$\sum_{m=1}^{2}\chi^{(m)}\frac{\mathrm{d}\phi^{(m)}}{\mathrm{d}t} = \frac{\partial\phi}{\partial t} - \delta_\Sigma\hat{\mathbf{w}}\cdot\sum_{m=1}^{2}\phi^{(m)}\hat{\mathbf{n}}^{(m)} + \mathbf{u}\cdot\left(\boldsymbol{\nabla}\phi + \delta_\Sigma\sum_{m=1}^{2}\phi^{(m)}\hat{\mathbf{n}}^{(m)}\right). \tag{B.2}$$

Appendix C. Transformation of volume and surface integrals

Appendix C.1. Reynolds transport theorem

Theorem 2 (Reynolds transport theorem)**.** *Let $\phi^{(m)} \in \mathcal{C}^1\left(\mathbb{R}^3 \times \mathbb{R}\right)$, and $V^{(m)}(t) \subset \mathbb{R}^3$ a volume delimited by a closed smooth surface $\partial(V^{(m)})(t)$. The velocity of the surface $\partial(V^{(m)})(t)$ is noted $\mathbf{w}^{(m)}$, and the normal vector to $\partial(V^{(m)})$ oriented outwards from $V^{(m)}$ is noted $\mathbf{n}^{(m)}$. The following relation is true:*

$$\frac{\mathrm{d}}{\mathrm{d}t}\int_{V^{(m)}}\phi^{(m)}\mathrm{d}^3V = \int_{V^{(m)}}\frac{\partial\phi^{(m)}}{\partial t}\mathrm{d}^3V + \int_{\partial(V^{(m)})}\phi^{(m)}\mathbf{w}^{(m)}\cdot\mathbf{n}^{(m)}\mathrm{d}^2S$$

Appendix C.2. Integral theorems for surfaces

In many occasions, it is necessary to interchange the differential and integral operators in expressions of the type:

$$\frac{\mathrm{d}}{\mathrm{d}t}\int_{\mathcal{S}}\hat{\phi}\mathrm{d}^2S. \tag{C.1}$$

This operation is enabled by the following theorem:

Theorem 3 (Transport theorem for surfaces [4, 49])**.** *Let $\mathcal{S}$ be a portion of the interface Σ. Let $\hat{\phi}$ a scalar field defined over the interface Σ. Under conditions of sufficient regularity, the following relation holds*

$$\frac{\mathrm{d}}{\mathrm{d}t}\left(\int_{\mathcal{S}}\hat{\phi}\mathrm{d}^2S\right)=\int_{\mathcal{S}}\left(\frac{\mathrm{d}\hat{\phi}}{\mathrm{d}t}+\hat{\phi}\boldsymbol{\nabla}_\Sigma\cdot\hat{\mathbf{w}}\right)\mathrm{d}^2S \tag{C.2}$$

where $\frac{\mathrm{d}\hat{\phi}}{\mathrm{d}t}$ is the derivative along the interface motion of the surface field $\hat{\phi}$ and $\boldsymbol{\nabla}_\Sigma\cdot\hat{\mathbf{w}}$ is the surface divergence of the interface velocity $\hat{\mathbf{w}}$.

It will also be useful to transform integrals on a closed contour into surface integrals. This is enabled by the next theorem.

Theorem 4 (Gauss theorems for surfaces [4, 49])**.** *Let $\mathcal{S}$ be a surface delimited by a closed contour $\mathcal{C}$. Let*

- *$\hat{J}$ a scalar field defined over the surface $\mathcal{S}$.*
- *$\hat{\mathbf{J}}$ a vector field defined over the surface $\mathcal{S}$ **and tangent to** $\mathcal{S}$.*

Under conditions of sufficient regularity, we have the relations

$$\oint_{\mathcal{C}}\hat{J}\hat{\mathbf{N}}\mathrm{d}l=\int_{\mathcal{S}}\left[\boldsymbol{\nabla}_\Sigma\hat{J}-(\boldsymbol{\nabla}_\Sigma\cdot\hat{\mathbf{n}})\,\hat{J}\hat{\mathbf{n}}\right]\mathrm{d}^2S \tag{C.3}$$

$$\oint_{\mathcal{C}}\hat{\mathbf{J}}\cdot\hat{\mathbf{N}}\mathrm{d}l=\int_{\mathcal{S}}\boldsymbol{\nabla}_\Sigma\cdot\hat{\mathbf{J}}\mathrm{d}^2S \tag{C.4}$$

where

- *$\boldsymbol{\nabla}_\Sigma\hat{J}$ is the surface gradient of the scalar field $\hat{J}$.*
- *$\boldsymbol{\nabla}_\Sigma\cdot$ is the surface divergence operator.*
- *$\hat{\mathbf{n}}$ is the normal vector to $\mathcal{S}$ (any orientation).*
- *$\hat{\mathbf{N}}$ is the vector normal to $\mathcal{C}$, tangent to $\mathcal{S}$ and directed outwards $\mathcal{S}$.*

References

[1] , . Doxygen documentation of Cantera 3.0.0: SurfPhase Class Reference. URL: `https://cantera.org/documentation/docs-3.0/doxygen/html/d2/d95/classCantera_1_1SurfPhase.html`.

[2] Aghalayam, P., Bui, P.A., Vlachos, D.G., 1998. The role of radical wall quenching in flame stability and wall heat flux: hydrogen-air mixtures. Combustion Theory and Modelling 2, 515–530. URL: `http://www.tandfonline.com/doi/abs/10.1088/1364-7830/2/4/010`, doi:doi: 10.1088/1364-7830/2/4/010.

[3] Appel, W., Kowalski, E., 2007. Mathematics for physics and physicists. Princeton University Press, Princeton, N.J. OCLC: ocm85773688.

[4] Aris, R., 1989. Vectors, tensors, and the basic equations of fluid mechanics. Dover books on engineering. dover ed ed., Dover Publications, New York.

[5] Bailera, M., Lisbona, P., Peña, B., Romeo, L.M., 2021. A review on CO2 mitigation in the Iron and Steel industry through Power to X processes. Journal of CO2 Utilization 46, 101456. URL: https://linkinghub.elsevier.com/retrieve/pii/S2212982021000238, doi:doi: 10.1016/j.jcou.2021.101456.

[6] Baltussen, M.W., Buist, K.A., Peters, E.A., Kuipers, J.A.M., 2018. Multiscale Modelling of Dense Gas–Particle Flows, in: Advances in Chemical Engineering. Elsevier. volume 53, pp. 1–52. URL: https://linkinghub.elsevier.com/retrieve/pii/S0065237718300103, doi:doi: 10.1016/bs.ache.2018.02.001.

[7] Breugem, W.P., 2012. A second-order accurate immersed boundary method for fully resolved simulations of particle-laden flows. Journal of Computational Physics 231, 4469–4498. URL: https://linkinghub.elsevier.com/retrieve/pii/S0021999112001374, doi:doi: 10.1016/j.jcp.2012.02.026.

[8] Caltagirone, J.P., Vincent, S., Caruyer, C., 2011. A multiphase compressible model for the simulation of multiphase flows. Computers & Fluids 50, 24–34. URL: https://linkinghub.elsevier.com/retrieve/pii/S004579301100199X, doi:doi: 10.1016/j.compfluid.2011.06.011.

[9] Chabane, A.M., Truffin, K., Nicolle, A., Nicoud, F., Cabrit, O., Angelberger, C., 2015. Direct Numerical Simulation of combustion near a carbonaceous surface in a quiescent flow. International Journal of Heat and Mass Transfer 84, 130–148. URL: https://linkinghub.elsevier.com/retrieve/pii/S0017931014011077, doi:doi: 10.1016/j.ijheatmasstransfer.2014.12.017.

[10] Chadil, M.A., Vincent, S., Estivalèzes, J.L., 2019a. Accurate estimate of drag forces using particle-resolved direct numerical simulations. Acta Mechanica 230, 569–595. URL: http://link.springer.com/10.1007/s00707-018-2305-1, doi:doi: 10.1007/s00707-018-2305-1.

[11] Chadil, M.A., Vincent, S., Estivalèzes, J.L., 2019b. Improvement of the Viscous Penalty Method for Particle-Resolved Simulations. Open Journal of Fluid Dynamics 09, 168–192. URL: http://www.scirp.org/journal/doi.aspx?DOI=10.4236/ojfd.2019.92012, doi:doi: 10.4236/ojfd.2019.92012.

[12] Chadil, M.A., Vincent, S., Estivalèzes, J.L., 2021. Gas-Solid Heat Transfer Computation from Particle-Resolved Direct Numerical Simulations. Fluids 7, 15. URL: https://www.mdpi.com/2311-5521/7/1/15, doi:doi: 10.3390/fluids7010015.

[13] Coltrin, M., Kee, R., Rupley, F., Meeks, E., 1996. SURFACE CHEMKIN-III: A Fortran package for analyzing heterogeneous chemical kinetics at a solid-surface - gas-phase interface. Technical Report SAND–96-8217, 481906. URL: http://www.osti.gov/servlets/purl/481906/, doi:doi: 10.2172/481906.

[14] Coltrin, M.E., Kee, R.J., Rupley, F.M., 1991. Surface chemkin: A general formalism and software for analyzing heterogeneous chemical kinetics at a gas-surface interface. International Journal of Chemical Kinetics 23, 1111–1128. URL: https://onlinelibrary.wiley.com/doi/10.1002/kin.550231205, doi:doi: 10.1002/kin.550231205.

[15] Cundall, P.A., Strack, O.D.L., 1979. A discrete numerical model for granular assemblies. Géotechnique 29, 47–65. URL: https://www.icevirtuallibrary.com/doi/10.1680/geot.1979.29.1.47, doi:doi: 10.1680/geot.1979.29.1.47.

[16] Deen, N.G., Peters, E., Padding, J.T., Kuipers, J., 2014. Review of direct numerical simulation of fluid–particle mass, momentum and heat transfer in dense gas–solid flows. Chemical Engineering Science 116, 710–724. URL: https://linkinghub.elsevier.com/retrieve/pii/S0009250914002656, doi:doi: 10.1016/j.ces.2014.05.039.

[17] Defay, R., Prigogine, I., Bellemans, A., 1966. Surface tension and adsorption. Longmans, London. OCLC: 1128032.

[18] Deising, D., Marschall, H., Bothe, D., 2016. A unified single-field model framework for Volume-Of-Fluid simulations of interfacial species transfer applied to bubbly flows. Chemical Engineering Science 139, 173–195. URL: https://linkinghub.elsevier.com/retrieve/pii/S0009250915004297, doi:doi: 10.1016/j.ces.2015.06.021.

[19] Delhaye, J.M., 1974. Jump conditions and entropy sources in two-phase systems. Local instant formulation. International Journal of Multiphase Flow 1, 395–409. URL: https://doi.org/10.1016/0301-9322(74)90012-3.

[20] Deutschmann, O. (Ed.), 2012. Modeling and simulation of heterogeneous catalytic reactions: from the molecular process to the technical system. Wiley-VCH, Weinheim.

[21] Fleckenstein, S., Bothe, D., 2015. A Volume-of-Fluid-based numerical method for multi-component mass transfer with local volume changes. Journal of Computational Physics 301, 35–58. URL: https://linkinghub.elsevier.com/retrieve/pii/S0021999115005306, doi:doi: 10.1016/j.jcp.2015.08.011.

[22] Gidaspow, D., 1994. Multiphase Flow and Fluidization: Continuum and Kinetic Theory Descriptions. Academic Press. Google-Books-ID: DTAFZ9rIfQwC.

[23] Giovangigli, V., 1999. Multicomponent Flow Modeling. Modeling and Simulation in Science, Engineering and Technology, Birkhäuser Boston, Boston, MA. URL: http://link.springer.com/10.1007/978-1-4612-1580-6, doi:doi: 10.1007/978-1-4612-1580-6.

[24] Glowinski, R., Pan, T.W., Hesla, T., Joseph, D., 1999. A distributed Lagrange multiplier/fictitious domain method for particulate flows. International Journal of Multiphase Flow 25, 755–794. URL: https://linkinghub.elsevier.com/retrieve/pii/S0301932298000482, doi:doi: 10.1016/S0301-9322(98)00048-2.

[25] Goodwin, D.G., Moffat, H.K., Schoegl, I., Speth, R.L., Weber, B.W., 2022. Cantera: An Object-oriented Software Toolkit for Chemical Kinetics, Thermodynamics, and Transport Processes. URL: https://zenodo.org/record/6387882, doi:doi: 10.5281/ZENODO.6387882.

[26] Hardy, B., Simonin, O., De Wilde, J., Winckelmans, G., 2022. Simulation of the flow past random arrays of spherical particles: Microstructure-based tensor quantities as a tool to predict fluid–particle forces. International Journal of Multiphase Flow 149, 103970. URL: https://linkinghub.elsevier.com/retrieve/pii/S0301932221003621, doi:doi: 10.1016/j.ijmultiphaseflow.2021.103970.

[27] Hoomans, B.P.B., Kuipers, J.A.M., Briels, W.J., van Swaaij, W.P.M., 1996. Discrete particle simulation of bubble and slug formation in a two-dimensional gas-fluidised bed: A hard-sphere approach. Chemical Engineering Science 51, 99–118. URL: https://linkinghub.elsevier.com/retrieve/pii/0009250995002715, doi:doi: 10.1016/0009-2509(95)00271-5.

[28] Ishii, M., Hibiki, T., 2011. Thermo-Fluid Dynamics of Two-Phase Flow. Springer New York, New York, NY. URL: http://link.springer.com/10.1007/978-1-4419-7985-8, doi:doi: 10.1007/978-1-4419-7985-8.

[29] Jakobsen, H.A., 2014. Chemical Reactor Modeling. Springer International Publishing, Cham. URL: http://link.springer.com/10.1007/978-3-319-05092-8, doi:doi: 10.1007/978-3-319-05092-8.

[30] Jenkins, J.T., Richman, M.W., 1986. Grad's 13-Moment System for a Dense Gas of Inelastic Spheres, in: The Breadth and Depth of Continuum Mechanics. Springer Berlin Heidelberg, Berlin, Heidelberg, pp. 647–669. URL: http://link.springer.com/10.1007/978-3-642-61634-1_31, doi:doi: 10.1007/978-3-642-61634-1_31.

[31] Jenkins, J.T., Savage, S.B., 1983. A theory for the rapid flow of identical, smooth, nearly elastic, spherical particles. Journal of Fluid Mechanics 130, 187. URL: http://www.journals.cambridge.org/abstract_S0022112083001044, doi:doi: 10.1017/S0022112083001044.

[32] Kataoka, I., 1986. Local instant formulation of two-phase flow. International Journal of Multiphase Flow 12, 745–758. URL: https://linkinghub.elsevier.com/retrieve/pii/0301932286900492, doi:doi: 10.1016/0301-9322(86)90049-2.

[33] Kataoka, I., Ishii, M., Serizawa, A., 1986. Local formulation and measurements of interfacial area concentration in two-phase flow. International Journal of Multiphase Flow 12, 505–529. URL: https://linkinghub.elsevier.com/retrieve/pii/0301932286900571, doi:doi: 10.1016/0301-9322(86)90057-1.

[34] Kee, R.J., Coltrin, M.E., Glarborg, P., Zhu, H., 2017. Chemically Reacting Flow: Theory, Modeling, and Simulation. Wiley. URL: http://doi.wiley.com/10.1002/9781119186304, doi:doi: 10.1002/9781119186304.

[35] Lyngfelt, A., Leckner, B., Mattisson, T., 2001. A fluidized-bed combustion process with inherent CO2 separation; application of chemical-looping combustion. Chemical Engineering Science 56, 3101–3113. URL: https://linkinghub.elsevier.com/retrieve/pii/S0009250901000070, doi:doi: 10.1016/S0009-2509(01)00007-0.

[36] Ma, C., Bothe, D., 2013. Numerical modeling of thermocapillary two-phase flows with evaporation using a two-scalar approach for heat transfer. Journal of Computational Physics 233, 552–573. URL: https://linkinghub.elsevier.com/retrieve/pii/S0021999112005426, doi:doi: 10.1016/j.jcp.2012.09.011.

[37] Maes, J., Soulaine, C., 2020. A unified single-field Volume-of-Fluid-based formulation for multicomponent interfacial transfer with local volume changes. Journal of Computational Physics 402, 109024. URL: https://linkinghub.elsevier.com/retrieve/pii/S0021999119307302, doi:doi: 10.1016/j.jcp.2019.109024.

[38] Maitri, R., Das, S., Kuipers, J., Padding, J., Peters, E., 2018. An improved ghost-cell sharp interface immersed boundary method with direct forcing for particle laden flows. Computers & Fluids 175, 111–128. URL: https://linkinghub.elsevier.com/retrieve/pii/S0045793018305401, doi:doi: 10.1016/j.compfluid.2018.08.018.

[39] Marschall, H., Hinterberger, K., Schüler, C., Habla, F., Hinrichsen, O., 2012. Numerical simulation of species transfer across fluid interfaces in free-surface flows using OpenFOAM. Chemical Engineering Science 78, 111–127. URL: https://linkinghub.elsevier.com/retrieve/pii/S0009250912001303, doi:doi: 10.1016/j.ces.2012.02.034.

[40] Maxey, M., 2017. Simulation Methods for Particulate Flows and Concentrated Suspensions. Annual Review of Fluid Mechanics 49, 171–193. URL: http://www.annualreviews.org/doi/10.1146/annurev-fluid-122414-034408, doi:doi: 10.1146/annurev-fluid-122414-034408.

[41] Müller, S., Theiss, L., Fleiß, B., Hammerschmid, M., Fuchs, J., Penthor, S., Rosenfeld, D.C., Lehner, M., Hofbauer, H., 2021. Dual fluidized bed based technologies for carbon dioxide reduction — example hot metal production. Biomass Conversion and Biorefinery 11, 159–168. URL: https://link.springer.com/10.1007/s13399-020-01021-4, doi:doi: 10.1007/s13399-020-01021-4.

[42] Nigmetova, A., Masi, E., Simonin, O., Dufresne, Y., Moureau, V., 2022. Three-dimensional DEM-CFD simulation of a lab-scale fluidized bed to support the development of two-fluid model approach. International Journal of Multiphase Flow 156, 104189. URL: https://linkinghub.elsevier.com/retrieve/pii/S0301932222001719, doi:doi: 10.1016/j.ijmultiphaseflow.2022.104189.

[43] Ozel, A., Brändle de Motta, J., Abbas, M., Fede, P., Masbernat, O., Vincent, S., Estivalezes, J.L., Simonin, O., 2017. Particle resolved direct numerical simulation of a liquid–solid fluidized bed: Comparison with experimental data. International Journal of Multiphase Flow 89, 228–240. URL: http://linkinghub.elsevier.com/retrieve/pii/S0301932216302221, doi:doi: 10.1016/j.ijmultiphaseflow.2016.10.013.

[44] Patankar, N., Joseph, D., 2001. Modeling and numerical simulation of particulate flows by the Eulerian–Lagrangian approach. International Journal of Multiphase Flow 27, 1659–1684. URL: https://linkinghub.elsevier.com/retrieve/pii/S0301932201000210, doi:doi: 10.1016/S0301-9322(01)00021-0.

[45] Poinsot, T., Veynante, D., 2011. Theoretical and numerical combustion. 3. ed ed., CNRS, Paris. OCLC: 775738742.

[46] Schneiders, L., Günther, C., Meinke, M., Schröder, W., 2016. An efficient conservative cut-cell method for rigid bodies interacting with viscous compressible flows. Journal of Computational Physics 311, 62–86. URL: https://linkinghub.elsevier.com/retrieve/pii/S0021999116000346, doi:doi: 10.1016/j.jcp.2016.01.026.

[47] Selçuk, C., Ghigo, A.R., Popinet, S., Wachs, A., 2021. A fictitious domain method with distributed Lagrange multipliers on adaptive quad/octrees for the direct numerical simulation of particle-laden flows. Journal of Computational Physics 430, 109954. URL: https://linkinghub.elsevier.com/retrieve/pii/S0021999120307282, doi:doi: 10.1016/j.jcp.2020.109954.

[48] Simonin, O., 2000. Statistical and continuum modelling of turbulent reactive particulate flows. Part 1: theoretical derivation of dispersed Eulerian modelling from probability density function kinetic equation, in: Theoretical and Experimental Modeling of Particulate Flows. von Karman Institute for Fluid Dynamics Rhode Saint Genèse (Belgium). Lecture Series.

[49] Slattery, J.C., Sagis, L.M., Oh, E.S., 2007. Interfacial transport phenomena. 2nd ed ed., Springer, New York.

[50] Snider, D.M., 2001. An Incompressible Three-Dimensional Multiphase Particle-in-Cell Model for Dense Particle Flows. Journal of Computational Physics 170, 523–549. URL: https://linkinghub.elsevier.com/retrieve/pii/S0021999101967476, doi:doi: 10.1006/jcph.2001.6747.

[51] Somorjai, G.A., Li, Y., 2010. Introduction to Surface Chemistry and Catalysis. John Wiley & Sons. Google-Books-ID: E7AfDCyfINYC.

[52] Thiam, E.I., Masi, E., Climent, E., Simonin, O., Vincent, S., 2019. Particle-resolved numerical simulations of the gas–solid heat transfer in arrays of random motionless particles. Acta Mechanica 230, 541–567. URL: http://link.springer.com/10.1007/s00707-018-2346-5, doi:doi: 10.1007/s00707-018-2346-5.

[53] Trujillo, M.F., 2021. Reexamining the one-fluid formulation for two-phase flows. International Journal of Multiphase Flow 141, 103672. URL: https://linkinghub.elsevier.com/retrieve/pii/S0301932221001208, doi:doi: 10.1016/j.ijmultiphaseflow.2021.103672.

[54] Tsuji, Y., Kawaguchi, T., Tanaka, T., 1993. Discrete particle simulation of two-dimensional fluidized bed. Powder Technology 77, 79–87. URL: https://linkinghub.elsevier.com/retrieve/pii/0032591093850107, doi:doi: 10.1016/0032-5910(93)85010-7.

[55] Tsuji, Y., Tanaka, T., Ishida, T., 1992. Lagrangian numerical simulation of plug flow of cohesionless particles in a horizontal pipe. Powder Technology 71, 239–250. URL: https://linkinghub.elsevier.com/retrieve/pii/003259109288030L, doi:doi: 10.1016/0032-5910(92)88030-L.

[56] Uhlmann, M., 2005. An immersed boundary method with direct forcing for the simulation of particulate flows. Journal of Computational Physics 209, 448–476. URL: https://linkinghub.elsevier.com/retrieve/pii/S0021999105001385, doi:doi: 10.1016/j.jcp.2005.03.017.

[57] Vincent, S., Bot, C.L., Sarret, F., Meillot, E., Caltagirone, J.P., Bianchi, L., 2015. Penalty and Eulerian–Lagrangian VOF methods for impact and solidification of metal droplets plasma spray process. Computers & Fluids 113, 32–41. URL: https://linkinghub.elsevier.com/retrieve/pii/S0045793014003995, doi:doi: 10.1016/j.compfluid.2014.10.004.

[58] Wachs, A., 2019. Particle-scale computational approaches to model dry and saturated granular flows of non-Brownian, non-cohesive, and non-spherical rigid bodies. Acta Mechanica 230, 1919–1980. URL: http://link.springer.com/10.1007/s00707-019-02389-9, doi:doi: 10.1007/s00707-019-02389-9.

[59] Wörner, M., Sabisch, W., Grötzbach, G., Cacuci, D.G., 2001. Volume-averaged conservation equations for volume-of-fluid interface tracking, New Orleans, Louisiana, USA. p. 12.